A Series Hybrid "Real Inertia" Energy Storage System

J. P. Rouse*[1], S. D. Garvey[1], B. Cárdenas[1] and T. R. Davenne[2]

[1]*Department of Mechanical, Materials and Manufacturing Engineering, University of Nottingham, Nottingham, Nottinghamshire, NG7 2RD, UK*
[2]*Rutherford Appleton Laboratory, Didcot, OX11 0QX, UK*

Abstract

The wide scale market penetration of numerous renewable energy technologies is dependent, at least in part, on developing reliable energy storage methods that can alleviate concerns over potentially interrupted and uncertain supplies. Many challenges need to be overcome, not least among them is allowing capacity for the wide range of time scales required to ensure grid stability. In thermal power plant, high frequency/short duration demand fluctuations, acting at the milliseconds to several seconds time scale, are addressed passively by the inertia of the grid. Here, grid inertia can be thought of as the mechanical inertia of spinning steel in steam and gas turbines. This allows time for active control measures to take effect at the tens of second to hours time scale and for the system to recover without a supply frequency deviation that is noticeable to the customer. It is of paramount importance that, as thermal plant is retired, renewable energy generation and storage systems account for the loss of this inertia. In the literature, strategies to address the loss of "real" inertia have often relied on emulation rather than actual replacement. The present work focuses on the preliminary development of a novel energy storage system that makes use of real inertia to address short term supply/demand imbalances while simultaneously allowing for extended depths of discharge. The concept looks to combine flywheel and compressed fluid energy stores in order to power a synchronous generator. By combining these energy storage technologies through a differential drive unit, DDU, it is anticipated that the benefits of high system inertia can be exploited in the short term while allowing energy to be continually extracted from the flywheel in the long term during storage discharge. The use of a DDU makes the present design particularly novel and distinct from other hybrid systems. In essence, this inclusion allows energy to be extracted entirely from the flywheel, inducing "real" inertia, or entirely from the secondary store, inducing "synthetic" inertia, or some combination of the two. Fundamental sizing calculations for a $50MW$ system with $20MWh$ of storage capacity are presented and used to design a suitable control system that allows for the operation of both primary flywheel and secondary compressed fluid energy stores. The transient behaviour of the system is simulated for several charge/discharge time profiles to demonstrate response stability for the system. Comments on system turnaround efficiency, which is dependent upon loading history but for the intended applications can be considered to be greater than 90% are also made here, along with a case study application to an isolated Californian solar powered grid.

Keywords: *Real Inertia, Hybrid Energy Storage, Kinetic Energy Storage, Frequency Response.*

1 Nomenclature

ω	Rotational speed (rad/s)
ω_{FW}	Flywheel rotational speed (rad/s)

*Corresponding Author - James Rouse, Department of Mechanical, Materials and Manufacturing Engineering, University of Nottingham, Nottingham, Nottinghamshire, NG7 2RD, UK. Email: James.Rouse@nottingham.ac.uk Tel: +44 (0)115 84 67683

$\hat{\omega}_{FW}$	Flywheel burst rotational speed (rad/s)
ω_D	Flywheel design rotational speed (rad/s)
ω_{SM}	Synchronous machine rotational speed (rad/s)
$\bar{\omega}_{SM}$	Synchronous machine nominal rotational speed (rad/s)
$\hat{\omega}_{SM}$	Synchronous machine target rotational speed (rad/s)
ω_{SMLL}	Synchronous machine rotational speed lower limit (rad/s)
ω_{SMUL}	Synchronous machine rotational speed upper limit (rad/s)
E_K	Kinetic energy (J)
ΔE_{FW}	Change in flywheel store energy (J)
ΔE_{HY}	Change in secondary store energy (J)
E_{Trans}	Transaction energy (J)
J	Moment of inertia ($kg.m^2$)
J_{FW}	Flywheel moment of inertia ($kg.m^2$)
J_{SM}	Synchronous machine moment of inertia ($kg.m^2$)
m	Flywheel mass (kg)
R_I	Internal flywheel radius, bore radius (m)
R_O	External flywheel radius (m)
R_{EP}	Elastic/plastic transition radius (m)
r	Radial coordinate (m)
ρ	Flywheel material density (kg/m^3)
σ_r	Radial stress component in flywheel (MPa)
σ_θ	Hoop stress component in flywheel (MPa)
A, B, C	Integration constants in flywheel stress expressions
σ_Y	Flywheel material yield stress (MPa)
σ_{UTS}	Flywheel material ultimate tensile strength (MPa)
$\Delta\sigma$	"Endurance" alternating stress, fully reversed condition (MPa)
σ_e	Flywheel material endurance limit (MPa)
S_A	Alternating stress for a particular loading condition (MPa)
S_M	Mean stress for a particular loading condition (MPa)
N_f	Number of cycles to failure
α, β	Basquin model parameters
p_i	Hydraulic fluid working pressure (bar)
ΔP	Hydraulic machine pressure differential (bar)
P_{Atmos}	Atmospheric pressure (bar)
p	Number of machine poles
f	Frequency (Hz)
G	Synchronous machine basic rating (MVA)
H	Synchronous machine inertia constant (MJ/MVA)
G_C	PID controller transfer function
K_P	Proportional gain ($kg.m^2/s$)
K_D	Differential gain ($kg.m^2$)
K_I	Integral gain ($kg.m^2/s^2$)
ω_n, ζ, k	DDU transfer function parameters
T	Instantaneous DDU torque (Nm)
T_R	DDU rated torque (Nm)
T_C	Controller torque (Nm)
T_W	Windage torque (Nm)
θ_{EM}	Electromechanical load angle (^{o})
$\hat{\theta}_{EM}$	Electromechanical load angle at rated synchronous machine power (10^o)
K_{SM}	Synchronous machine spring constant ($Nm/^o$)
err	Rotational speed error, difference between instantaneous synchronous machine speed and target speed (rad/s)
t	Simulation time (s)
t_s	Total simulation time (s)
P_{PV}	Photovoltaic cell power (MW)

P_{Demand}	Total demand power (MW)
P_{Gen}	Total generated power (MW)
P_{Base}	Total baseline power (MW)
$\hat{P}_{SM}$	Rated synchronous machine power (MW)
C_W	Windage loss coefficient
η_G	Generator efficiency
η_M	Motor efficiency
η_P	Pump efficiency
η_{PV}	Photovoltaic cell efficiency
η_{INV}	Inverter efficiency
η_T	Total system efficiency
h_{pv}, p_{pv}, q_{pv}, m_{pv}, r_{pv}, s_{pv}, u_{pv}	Photovoltaic cell model coefficients
θ_{PV}	Photovoltaic cell temperature (^oC)
θ_{Air}	Instantaneous air temperature (^oC)
$\hat{\theta}_{Air}$	Peak air temperature (^oC)
t_{rise}	Time of sunrise
t_{set}	Time of sunset
$t_{\hat{\theta}_{Air}}$	Time of peak air temperature
M_{Air}	Normalised air mass
G_{β}	Global solar irradiation (W/m^2)
ψ_Z	Zenith angle (^{o})
d_n	Day number
C_s, C_v, C_f	Hydraulic machine model coefficients
$Q_{P/M}$	Pump/motor flow rate (m^3/s)
$T_{P/M}$	Pump/motor torque (Nm)
D	Hydraulic machine displacement (cc/rev)
x	Hydraulic machine displacement fraction
A_L	Loading cycle amplitude (MW)
t_L	Loading cycle period (s)
$RoCoF$	Rate of change of (grid) frequency (Hz/s)

2 Introduction

The intermittent and irregular nature of renewable energy sources necessitates at least some form of energy storage if uninterrupted supply is to be achieved[1]. Mismatches in supply and demand need to be accounted for on a wide range of time scales, from the order of weeks or months as a result of diurnal and seasonal variations[2], to seconds and milliseconds . In order to ensure a stable grid, it is critically important that a balance is maintained between consumption and generation in real time over this wide range of time scales[3]. The inertia response of an energy system limits the rate of change of frequency, known as RoCoF, when a sudden change in load is encountered[3]. Systems such as thermal energy storage and pumped hydroelectric have very little associated inertia and may be thought of as providing slow response energy storage. Slow energy storage in the present context may be thought of as reactions to grid imbalances that take place over time periods greater than several minutes. Conversely, fast energy storage addresses momentary load imbalances on the millisecond to second time scale.

In thermal power plants, the inertia of a turbine passively controls the rate of the change in speed to the synchronous machine it is coupled to. This action buys time for active control systems to take effect and stabilise the system frequency by adjusting prime mover inputs. Note that prime mover adjustment may not be required for a particular load imbalance scenario if, for example, sufficient kinetic energy can be extracted from synchronous machine rotors. Renewable energy sources on the other hand are commonly connected to the grid via power converters rather than synchronous generators. As such they operate to generate maximum available power and do not respond to system load directly . Power converters require control technology in order to keep line frequencies, voltages and power oscillations within acceptable tolerances while also guarding against power circulation[4]. Renewable energy sources typically have little in the way of intrinsic inertia in the first instance. Wind turbines (for

example), have relatively low inertia constants, $2-6s$[5], and it is debatable as to whether or not this inertia is truly seen by the grid due to the interconnecting power electronics. For comparison, turbo generators used in conventional steam power plants have inertia constants of $7-9s$[6]. Inertia constants may be expressed as the ratio of stored kinetic energy in a system, rotating at rated speed, to the rated electrical power of the system. Inertia constants have time units and indicate how long it would take for a rotating mass to de-accelerate to stationary if continuously discharged at rated power[6].

The present work proposes an electricity in/electricity out (EIEO) storage system that bridges the gap between the extremes of energy storage time scales, with sudden load imbalances addressed through the introduction of "real system inertia" (in a flywheel) and secondary energy stores (compressed fluid) exploited for sustained delivery over longer time periods. Real inertia is distinct to emulated or synthetic inertia, and may be thought of as energy storage that acts in an entirely passive manner. That is to say, the transfer of energy is determined completely by the reluctance of the system to change speed. By way of example, a $50MW$ system with a capacity of $20MWh$ is sized here with the view that such a design could form part of the energy storage requirement for an offshore wind farm.

Numerous techniques have been proposed for emulating inertia in renewable generators[7, 8]. For example, offshore wind farms (particularly in remote locations) are often connected to the grid through high voltage DC (HVDC) links, thereby decoupling offshore frequency fluctuations from grid fluctuations. Several articles have been published that detail methods for inertia emulation in such systems using, say, capacitance within the HVDC[9, 10]. The system presented here uses only a minimum amount of voltage regulation electronics, similar to that which is deployed on thermal power plant synchronous machines.

Several hybrid energy storage systems that employ a flywheel have been proposed in the literature with a renewable energy (particularly wind) emphasis. The work of Prodromidis and Coutelieris[11, 12], for example, has detailed experimental investigations into flywheel energy store design/efficiency and the application of hybrid battery/flywheel standalone systems to small grids. In the former study steel and aluminium flywheel designs, which utilised different cross section geometries, were compared at the laboratory scale ($0.7kW$ and $0.2Wh$) for building energy storage applications. Aluminium designs were favoured due to the possibility for greater levels of energy storage in the given application, however interactions with a grid were not considered and their system only has a limited relevance to the one proposed in the present work. Combined battery and flywheel hybrid energy stores were also analysed by Prodromidis and Coutelieris for a standalone system on the Greek island of Naxos. Specifically, flywheels were used to supplement the energy storage of Hoppecke, Surrette, and Vision batteries, all with approximately $3000Ah$ of storage. Such capacity levels were chosen so that the considered systems could feasibly supply a typical house. Net present costs of the flywheel and battery systems were comparable to simple battery systems (approximately \$6000). Again however, the systems considered in Prodromidis and Coutelieris' work did not interact directly with any kind of grid and were sized at a vastly different scales to the system proposed in the present work.

Sebastián and Peña-Alzola[13] focused on the development of a control system and simulation method for a flywheel energy store which was to be used alongside a hybrid wind/diesel power systems. The flywheel component was sized using elastic stress analysis and a Tresca failure criterion (a similar study will be carried out later in this paper). Machine and grid side control systems were established in order to maintain link voltages by varying the low speed flywheel power, thereby resulting in smoother operation during power transients. The system considered in this work was however limited to isolated micro-grid applications, with power/capacity ratings of approximately $150kW$ and $5\times10^{-3}MWh$, respectively.

Of particular interest here are publications by Carrillo, Feijóo and Cidrás[14], where synchronous and asynchronous machines were attached to diesel generators and flywheel systems in order to compare their performance in supplementing wind power in isolated locations (i.e. for low power applications of approximately $50kW$). Building on the author's previous work, one synchronous machine/flywheel configuration featured a hydraulic transmission linking the two components. This was done in order to "allow energy transfer between two systems rotating at different speeds". During discharge, the flywheel would be spun down and used to drive a fixed displacement pump that circulates a pressurised fluid in line connected to a variable displacement motor. Work can thus be extracted by a motor to power a synchronous machine. Broadly speaking, variable speed configurations (asynchronous machines) were concluded to be superior for accommodating wind speed fluctuations and synchronous machines were better for demand load variations. The benefits of matching demand variations are still evident in the

synchronous system proposed here, however potentially significant losses associated with the presence of two hydraulic pump/motor assemblies are avoided and a stiffer (solid) link is provided between the main source of inertia (the flywheel) and the synchronous machine.

Flywheel energy stores have historically been widely used for un-interruptible power supply (UPS) applications[15] and have had a great deal of success in this area with many manufacturers in the market[16]. 97% of AC outages are resolved in under 3s[16], suggesting that high cycle lives are highly valuable and limiting the effectiveness of electrochemical energy storage solutions. Diesel generator/flywheel UPS systems may be considered "series" energy stores (see section 3) in a similar sense to the hybrid system developed in the present work. It should be noted however that, in the system developed here, it is possible to fully decouple to flywheel from the synchronous machine and supply power solely from some secondary source.

3 Series Hybrid Kinetic Energy Storage (SHyKESS)

The presented hybrid energy storage system, refereed to as SHyKESS, falls into a category of systems that the authors would term "series" type systems. These are distinct to "parallel" type systems, which make up the vast majority of designs proposed in the literature. In parallel systems, energy storage technologies are individual elements feeding a common bus linked to the grid. This type of hybrid system is considered the norm. The overview of energy store hybrids in papers by Amrouche et al.[17] and Bocklisch[18] highlight this fact and little exploration into alternative areas can be found in the literature. The complexity of parallel hybrid designs is only increased when it is remembered that each generator must be controlled by some overarching, ideally autonomous, system that is sensitive to the various supply and demand scenarios that a grid may experience. See, for example, the work of Shankar and Mukherjee[19] and Hamzaoui et al.[20]. The proposed system may be termed a "series" hybrid energy storage system. Electrical power to the grid is supplied by a single generator (per base unit) which categorically generates in a synchronous manner, thereby removing the need for frequency control power electronics. The grid "sees" precisely the same type of generator that one would expect from a conventional fossil fuel power plant. Furthermore, the proposed hybrid allows energy to be stored and extracted from multiple stores simultaneously at rates that are appropriate for the specific grid condition. In the case of a system demand for example, short term generation can be provided by running down a flywheel. If prolonged energy recovery is required the generator still runs at a synchronous speed by extracting energy from both the flywheel and a compressed fluid store. The ratio of power from the flywheel to the power from the compressed fluid would clearly decreases as the flywheel spins down. SHyKESS comprises of several simple components and, during charge/discharge cycles, can be thought to operate in one of several modes. For clarity, an overview of the SHyKESS system is presented here with a step by step discussion of a typical operation pattern.

An overview of SHyKESS is given in figure 1. A synchronous machine (item 4) is connected to a flywheel (item 1) through a differential drive unit (DDU, item 3). In the present work, the DDU may most readily be interpreted as a hydraulic pump/motor, the rotor of which is connected directly to the synchronous machine and the "stator" of which is connected to the flywheel shaft. Clearly, if no fluid is allowed to flow through such a machine, the pump/motor assembly will act as a rigid coupling. If fluid is however allowed to flow through the machine the synchronous machine shaft will spin relative to the flywheel shaft, thereby offering a path for the introduction of "slip" energy into the system. Both the synchronous machine and flywheel are mounted on hollow shafts. These are connected only through the DDU and allow for the transmission of high pressure compressed fluid (the secondary energy store). It is important to note that this feature of SHyKESS facilitates one of the system's key advantages over other proposals. From a mechanical perspective (i.e. in terms of torque transmission), none of the components are grounded to earth. Torque transmission is accomplished through the DDU, the casing of which is free to rotate with, say, the synchronous machine rotor. The DDU allows slip between the flywheel and synchronous machine rotor speeds and houses a variable displacement compressed fluid machine. This machine may operate as a motor (during system discharge, thereby extracting energy from the compressed fluid store) or as a pump (allowing for charging of the secondary energy store). A sprag clutch is incorporated in the coupling between the flywheel and DDU in order to prevent the flywheel's direction of rotation being reversed during full discharge (i.e. when the speed of the flywheel relative to ground is 0). There is a subtlety in the design of the synchronous machine that results from

the use of a hollow rotor shaft. A 4 pole design is favoured over a 2 pole variant as it is expected that this will minimise disturbances to the magnetic field which, in the 2 pole machine must pass through changing media, namely the steel rotor shaft and the internal compressed fluid.

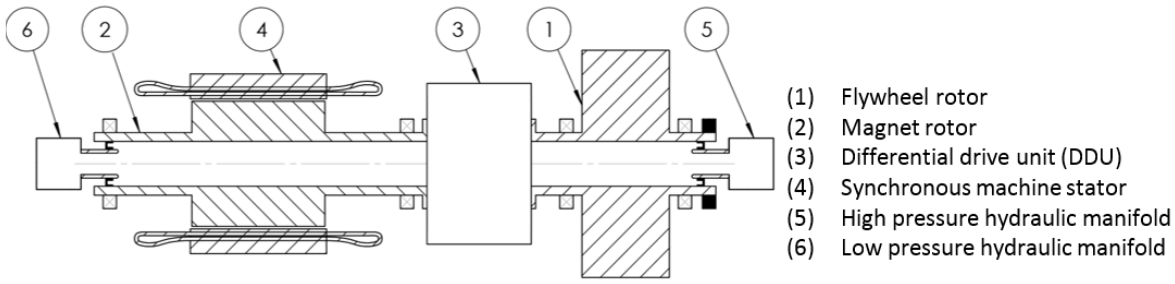

Figure 1: The proposed flywheel based energy storage concept SHyKESS (Series Hybrid Kinetic Energy Storage System). Note that, in the present work, the DDU may be through of as a hydraulic motor/pump assembly.

The multiple operating modes of SHyKESS are explained in the flowchart given in figure 2. Figure 3 shows a schematic representation of how contributions to total power are made from the flywheel and secondary energy stores as the flywheel speed, ω_{FW}, varies from the nominal synchronous machine speed, $\bar{\omega}_{SM}$, to 0 (relative to earth). Both charging and discharging operating conditions are represented. Consider SHyKESS in mode 1, where both the flywheel and synchronous machine rotor are rotating at the same speed. Note that, $\omega_{FW} = \omega_{SM}$, where ω_{FW} and ω_{SM} are the flywheel and synchronous machine rotational speeds, respectively. For the purposes of this example, we shall assume that this is the synchronous speed ($50\pi rad/s$ for a 4 pole machine) and initially there is no load on the system. During discharge, when the synchronous machine acts as a generator, the DDU is initially locked and the system has the sum of flywheel and rotor inertias. As the system continues to discharge ω_{SM} will approach a lower limit, ω_{SMLL}, which is the minimum speed the synchronous machine can run such that generated frequency is within the grid tolerance. Note that in the UK, the 2002 electricity safety, quality and continuity regulations (ESQCR 2002) stipulate that frequency must be with $\pm 1\%$ of the nominal operating frequency (in this case $50Hz$)[21]. When this limit is reached, the DDU will unlock, allowing an amount of slip between ω_{FW} and ω_{SM} (during discharge, this is mode 2A). In this example, energy is extracted from the secondary (compressed fluid) store in order to maintain a constant torque over the DDU, acting to slow down the flywheel (thereby extracting stored kinetic energy) and return the rotor speed to the target (synchronous) speed ($\hat{\omega}_{SM}$)). This condition is represented in figure 3 a). Note that, as the flywheel speed approaches 0, the secondary energy store accounts for a greater contribution to the total power. Control of a variable displacement motor in the DDU can therefore be achieved by comparing ω_{SM} to $\hat{\omega}_{SM}$) (thereby modifying an output torque). Power can continue to be supplied by the flywheel until its rotational speed (relative to ground) becomes 0 and the sprag clutch disengages (mode 3A).

In the case of charging (starting in mode 3A), the DDU acts as a pump, thereby providing a negative torque to the synchronous machine rotor in an attempt to slow it down. As such the sprag clutch will re-engage and the speed of the flywheel will increase (mode 2A). With continued charging of the system the speed of the flywheel will continue to increase and approach the speed of the synchronous machine. The charging condition is represented in figure 3 b). At this point the DDU will lock and the system will move back into mode 1. The shaft speed (identical to the flywheel and synchronous rotor speed in this case) will now increase until it reaches the upper tolerance limit for the machine (ω_{SMUL}). At this point the DDU will again unlock, with the secondary store drive acting as a motor (spinning in the opposite direct to the charging instance) to increase the flywheel speed while keeping the synchronous machine speed within tolerance (mode 2B). By doing this we may increase the amount of energy stored in the flywheel, however a strucutral limit will exist which prohibits any more being stored in the system (mode 3B). At this point a secondary (separate) store must be employed. The above example is demonstrated using a transient response model in section 5 (figure 7).

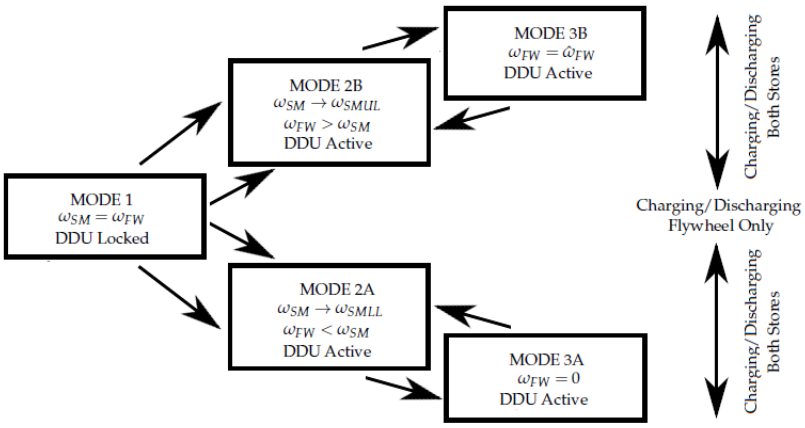

Figure 2: SHyKESS operating mode flowchart.

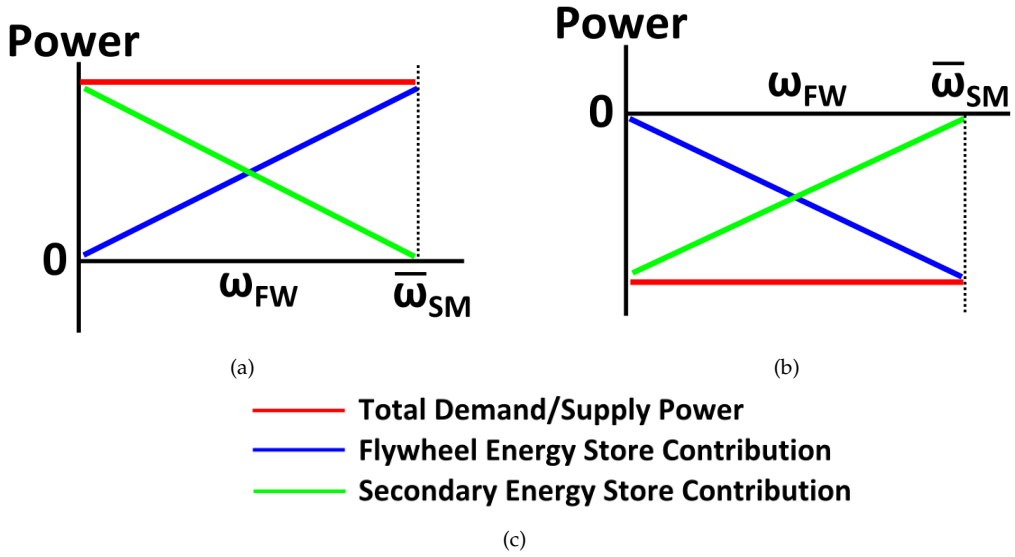

Figure 3: Schematic representations of power contributions for the SHyKESS system under (a) discharging and (b) charging operating conditions.

4 SHyKESS Basic Design Calculations and Development of a Control System Model

To make a true impact on the energy market high power designs are required. The present work will therefore focus on the development of a $50MW$ $20MW.hr$ capacity system, meaning that contributions comparable to hydro-storage can be made realised[22] and the system would be well suited for offshore wind applications. What follows are fundamental sizing calculations for the $50MW$ system and the development of a transient response model.

The kinetic energy (E_K) stored in a flywheel may be given by equation (1), where J is the moment of inertia (see equation (2)). Note m is flywheel mass, R_I/R_O are the internal and external radii, respectively, and ω is the flywheel's rotational velocity. A 4 pole synchronous machine is to be implemented (for the reasons given in the previous section), giving rise to a synchronous rotational velocity of $50\pi rad/s$ ($\omega_{SM} = (4\pi f)/p$, where p is the number of poles in the machine and f is the operating frequency, here taken to be $50Hz$). Using the requirement for a $20MW.hr$ storage capacity and equation (1), it can be found that the SHyKESS flywheel requires a moment of inertia of $J_{FW} = 5.836x10^6 kg.m^2$.

$$E_K = \frac{1}{2} J_{FW} \omega^2 \tag{1}$$

$$J_{FW} = \frac{1}{2} m (R_O^2 + R_I^2) \tag{2}$$

The inertia of a synchronous machine rotor may be approximated in the following way (taken from Kothari and Nagrath[6]). Equation (3) relates G, the machine base rating (MVA) and a machine based inertia constant H (MJ/MVA, note therefore that GH is equivalent to the rotor's kinetic energy) to M_e (the moment of inertia of the rotor based on the electrical field rotational velocity ω_s, $MJ.s/rad(electrcial)$). The relationship between ω_s ($rad(electrical)/s$) and ω_{SM} ($rad(mechanical)/s$) is given in equation (4) for a machine with p poles. Using equations (3) and (4), the definition of kinetic energy in equation (1) and assuming $H = 6MJ/MVA$ (which is representative of a condensing turbine steam generator), $J_{SM} = 24.317x10^3 kg.m^2$.

$$GH = \frac{1}{2} M_e \omega_s \tag{3}$$

$$\omega_s = \left(\frac{p}{2}\right) \omega_{SM} \tag{4}$$

Assuming a constant thickness flywheel design, the optimum solution in terms of packaging and resource usage of the flywheel mass is dependent on setting a burst speed ($\hat{\omega}_{FW}$). This, in turn, is dependent on accurately estimating the stress distribution in the flywheel. Elastic solutions for the radial and hoop stresses (σ_r and σ_θ, respectively) in a rotating disc are widely known (see equations (5) and (6), where B and C are constants of integration) but would only allow for very conservative designs (i.e. those that deploy mass poorly) to be realised. This is particularly true for the present case, where the presence of an internal bore (for the compressed fluid supply) results in a stress riser at the internal radius. Given the hardening characteristics of many engineering steels, the complete avoidance of yielding is unreasonable for a large number of engineering applications and it is the author's assertion that SHyKESS is one of them.

$$\sigma_r = B - \frac{C}{r^2} - \frac{\rho \omega^2 (3+\nu)}{8} r^2 \tag{5}$$

$$\sigma_\theta = B + \frac{C}{r^2} - \frac{\rho \omega^2 (1+3\nu)}{8} r^2 \tag{6}$$

Before sizing the hollow flywheel an estimation of the internal bore radius (R_I) is required. This is constrained by the flow of fluid in the secondary store. ISO VG150 oil is taken as the secondary store working fluid ($\nu_{oil} \approx 7.0 \times 10^{-4} m^2/s$ and $\rho_{oil} \approx 870 kg/m^3$[23]) and a pressure differential over the DDU of $20MPa$ is assumed. Using this pressure differential and the required machine power, $50MW$, the rated flow rate for the machine can be calculated, namely $1.0x10^5 cc/rev$ at synchronous speed. Assuming a uniform velocity profile and imposing a laminar flow condition consequently indicates that $R_I = 0.4m$.

In the present work, flywheel sizing is based on elastic-perfectly-plastic (EPP) material assumptions with a Tresca yield criterion. Note that this solution is well established (see Rees[24, 25]) and only a brief overview is given here. Attentional is focused on solutions for non-zero σ_r values at the internal bore. Equation (7) describes equilibrium in a disc rotating at speed ω, where ρ is the material density and r is the radial coordinate, assuming plane stress conditions. It is expected that casting a flywheel of the dimensions discussed here as a single entity will afford many non-trivial challenges for both manufacture and transport. As such, it is expected that the present work's flywheel will be made up of several laminates or plates which are constrained axially. As such, the plane stress conditions assumed here are taken to be valid. The limiting case (burst) is considered to be when the material has yielded through the entire radius of the flywheel. The Tresca criterion and EPP material assumption therefore indicate that this occurs when $\sigma_\theta = \sigma_Y$ for all r. Substituting this in equation (7) and integrating gives equation (8), where the constant A is determined using the boundary condition at $r = R_I$, namely $\sigma_r = -p_i$, the internal shaft pressure (see equation (9)). With this in hand, the external flywheel radius

R_O may be found at a design speed, ω_D, which gives rise to a completely plastic flywheel by enforcing the external boundary condition ($\sigma_r = 0$ at $r = R_O$). For SHyKESS using EN24 (BS 970 817M40) steel ($\sigma_Y = 940MPa$, $\rho = 8170kg/m^3$[26]), it may be found that $R_O = 3.18m$. Using equation (2), the length of the flywheel (L) may be found to be $4.45m$. As the Tresca criterion is already conservative it is assumed here that ω_D need only marginally greater than the maximum flywheel operational speed ($\hat{\omega}_{FW}$). For the purposes of the present study, $\omega_D = 1.1\omega_{SM}$ and $\hat{\omega}_{FW} = 1.04\omega_{SM}$. Fully plastic flywheel stress distributions (i.e. when $\omega = \omega_D$) can be seen in figure 4 (a). When $\omega \leq \omega_D$ stresses will transition from plastic (towards the centre of the flywheel) to elastic at some radial position R_{EP}. Solutions in these two regions are given by equation (8) and equations (5) and (6), respectively. R_{EP} may be found by enforcing continuity in σ_r over this boundary. Elastic/plastic stress distributions for $\omega = \hat{\omega}_{FW}$ are presented in figure 4 (b) (note R_{EP} is indicated by a dashed vertical line).

$$\sigma_\theta - \sigma_r - r\frac{d\sigma_r}{dr} = \rho r^2\omega^2 \tag{7}$$

$$\sigma_r = \sigma_Y - \frac{\rho r^2\omega^2}{3} + \frac{A}{r} \tag{8}$$

$$A = -R_I\left(p_i + \sigma_Y - \frac{\rho {R_I}^2\omega_D^2}{3}\right) \tag{9}$$

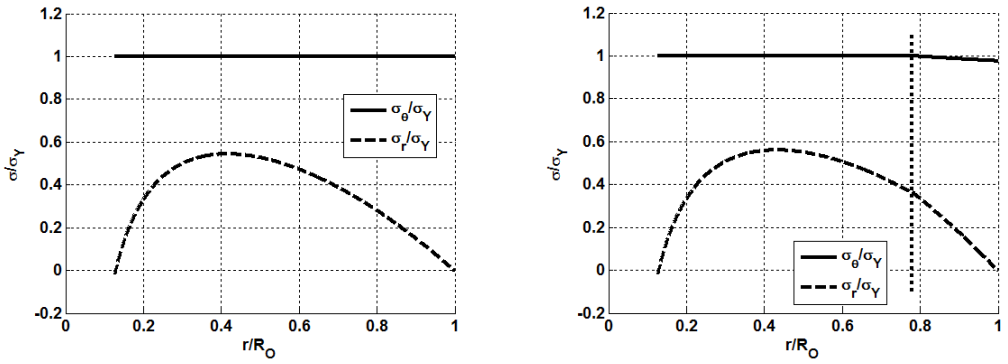

(a) (b)

Figure 4: Normalised flywheel stress distributions for (a) the design speed case (ω_D) and (b) the maximum operating speed case ($\hat{\omega}_{FW}$).

With the basic dimensions fo the system in place, attention can be focused on a simple controller that limits the shaft torque through the DDU in modes 2A and 2B. For convenience, equations presented here will be given in the Laplace domain. A PID controller has been applied ($G_C = K_P + K_D s + K_I/s$) that acts on the error (err, see figure 5) between the instantaneous synchronous machine speed (ω_{SM}) and the desired value ($\bar{\omega}_{SM}$, in the present work equal to $50\pi rad/s$) in order to control the shaft torque over the DDU (T_C in figure 5) and hence regulate power from the secondary store. This system may be visualised through the block diagram in figure 5. The high frequency response of the DDU is simulated by a second order damped linear system (P_1), of the form given in equation (10). Values for ω_n, ζ and k ($100Hz$, 0.3142 and 1, respectively) were chosen to give a unity response at low frequency (i.e. at low frequency $T_C = T$) while allowing for the possibility of resonance in the DDU at a realistic natural frequency.

Load angle (sometimes called torque angle) is defined as the angle between the rotor's magneto-motive force (mmf) and the resultant mmf[27]. This quantity is used here to simulate a first order approximation of the mechanical load exerted on SHyKESS (T_{Load} in figure 5). Grid load will, in the next section, be approximated by varying the load angle (θ_{EM}), with the associated torque determined by approximating the synchronous machine as a rotational spring with constant K_{SM}. Assuming a 10^o load angle at rated torque, K_{SM} can be estimated as $31831Nm/^o$ for the presented design. In practice,

reactive power would be balanced by adjusting the machine's field strength, in effect altering the value of K_{SM}, however this is not considered in the present work. The difference in DDU torque and grid load "torque" is integrated in P_2 in order to determine the synchronous machine speed ($P_2 = 1/J_{SM}s$). Note that flywheel speed is omitted from figure 5 as the DDU is only concerned with controlling ω_{SM}. The negative of the DDU torque can of course be integrated in order to determine ω_{FW}.

Analysis of the block diagram allows for two transfer functions to be defined (G_1 and G_2) such that $\bar{\omega}_{SM}(s)G_1 - \theta_{EM}(s)G_2 = \omega_{SM}(s)$, where G_1 and G_2 are given in equations (11) and (12), respectively. The Routh-Hurwitz stability criterion may be applied in order to constrain the PID gains in G_C (see equation (13)), however a far more useful condition for K_D is found through inspection of the system. It is clear that $\dot{err} = -\dot{\omega_{SM}}$ and it is intended that the DDU in modes 2A and 2B should replicate the flywheel inertia. If this is to be achieved, we may say that $K_D = J_{FW}(kg.m^2)$. Using this condition, the Routh-Hurwitz result and by testing candidate K_P and K_I values for benchmark charge/discharge cases (see section 5), the following gains may be determined for the presented SHyKESS configuration; $K_P = 1.0x10^5(kg.m^2.s^{-1})$ and $K_I = 2.0x10^5(kg.m^2.s^{-2})$.

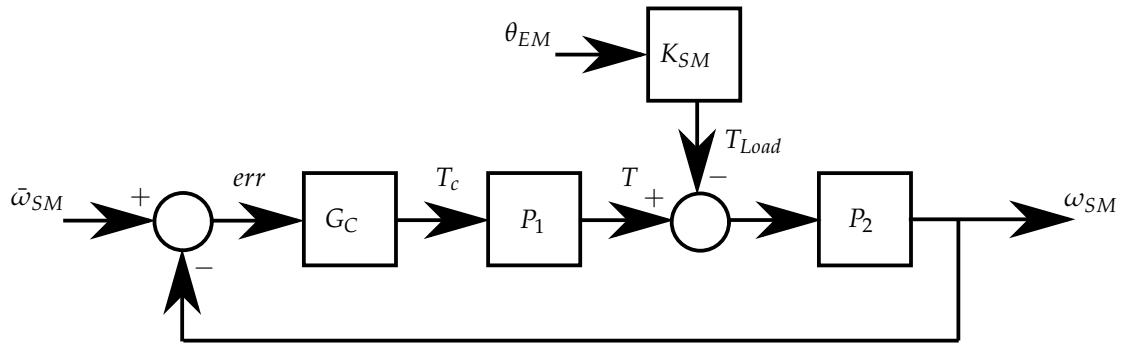

Figure 5: Block diagram for the control of ω_{SM} in mode 2A and 2B.

$$P_1 = \frac{\omega_n^2/k}{s^2 + \zeta 2\omega_n s + \omega_n^2} \tag{10}$$

$$G_1 = \frac{G_C P_1 P_2}{1 + G_C P_1 P_2} \tag{11}$$

$$G_2 = \frac{K_{SM} P_2}{1 + G_C P_1 P_2} = \frac{K_{SM}\left(Ms^3 + Cs^2 + Ks\right)}{J_{SM}s\left(Ms^3 + Cs^2 + Ks\right) + K_D s^2 + K_P s + K_I} \tag{12}$$

$$K_D > \frac{M}{C}K_P - J_{SM}, \qquad K_D + J_{SM} > CJ_S M\frac{K_I}{K_P} + \frac{M}{C}K_P \tag{13}$$

5 SHyKESS Transient Behaviour

Simulations have been completed using the model developed in section 4 for several loading scenarios in order to a). suggest appropriate controller gain values and b). to illustrate the transient response of SHyKESS as it switches between different modes of operation. Solutions were found in the time domain using Matlab's ODE23tb solver and were verified against Simulink results for simulations performed in isolation (i.e. for limited periods of time in a single mode of operation). In all plots and for the sake of clarity, normalised values of ω_{SM}, ω_{FW}, T (the torque transmitted across the DDU) and θ_{EM} (defined by the particular loading condition) are presented over a normalised time period (t/t_s, where t_s is the total

simulation time). Note that normalisation factors are $\bar{\omega}_{SM}$, T_R (the hydraulic machine rated torque) and $\hat{\theta}_{EM}$ (the assumed load angle at rated power, here 10^o).

The partial discharge of the system under constant system load is shown in figure 6. Point A in this figure indicates the transition between system modes 1 and 2A (prior to this point $\omega_{SM} = \omega_{FW}$). Discharging is continued at constant load in figure 7 until point B, where the flywheel speed is 0 (relative to ground) and the system enters mode 3A. Charging of the system commences at point C (mode 2A, represented by a negative load angle), causing an increase in ω_{FW} until this speed locks back into ω_{SM} at point D. The flywheel continues to be charged until point E (where $\omega_{SM} \rightarrow \omega_{SMUL}$), meaning that the DDU is once again unlocked. At point F $\omega_{FW} = \hat{\omega}_F W$ and the system is saturated (mode 3B).

Step changes in load have been applied during modes 1 and 2 in figures 8 to 9 in order to demonstrate stability in the system. In all cases, $\omega_{SMLL} < \omega_{SM} < \omega_{SMUL}$ (i.e. $\pm 1\% \omega_{SM}$). Note that the load perturbation in figure 8 takes place during mode 1 operation, therefore control is achieved entirely passively (due to the high inertia of the system) and the DDU does not unlock until $\omega_{SM} \rightarrow \omega_{SMLL}$.

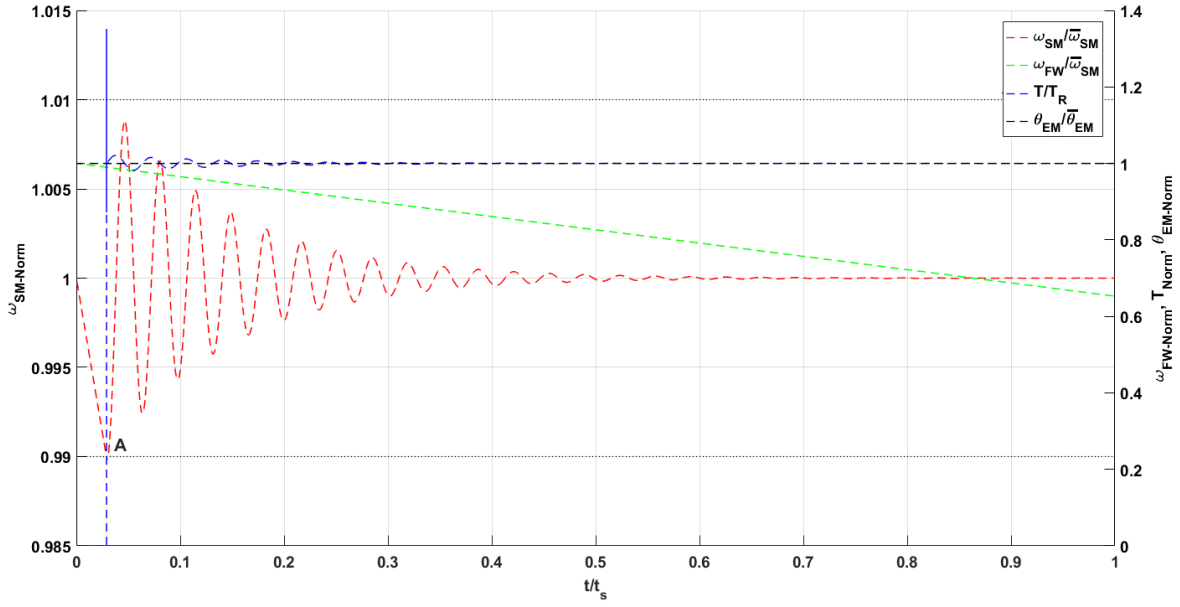

Figure 6: SHyKESS transient response during constant load discharge (partial discharge of the flywheel and secondary store). Note that $t_s = 3000s$.

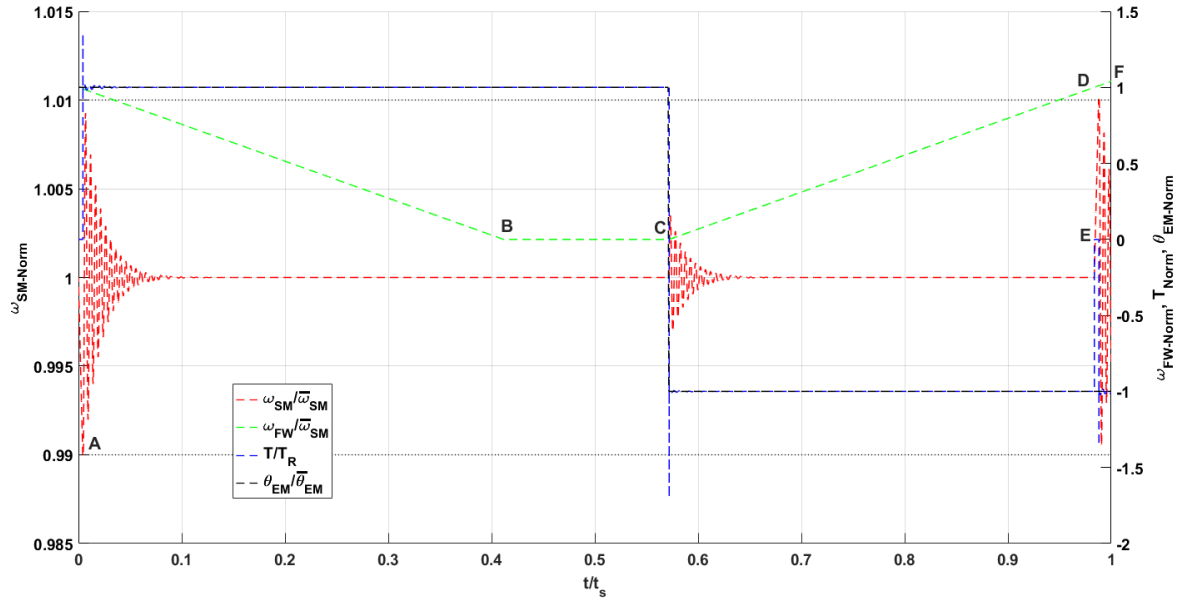

Figure 7: SHyKESS transient response during a discharge/charge cycle, highlighting the re-locking of the DDU (moving from mode 2A to 1 during charging, point E) and flywheel overspeed protection (mode 3B, point F). Note that $t_s = 7000s$.

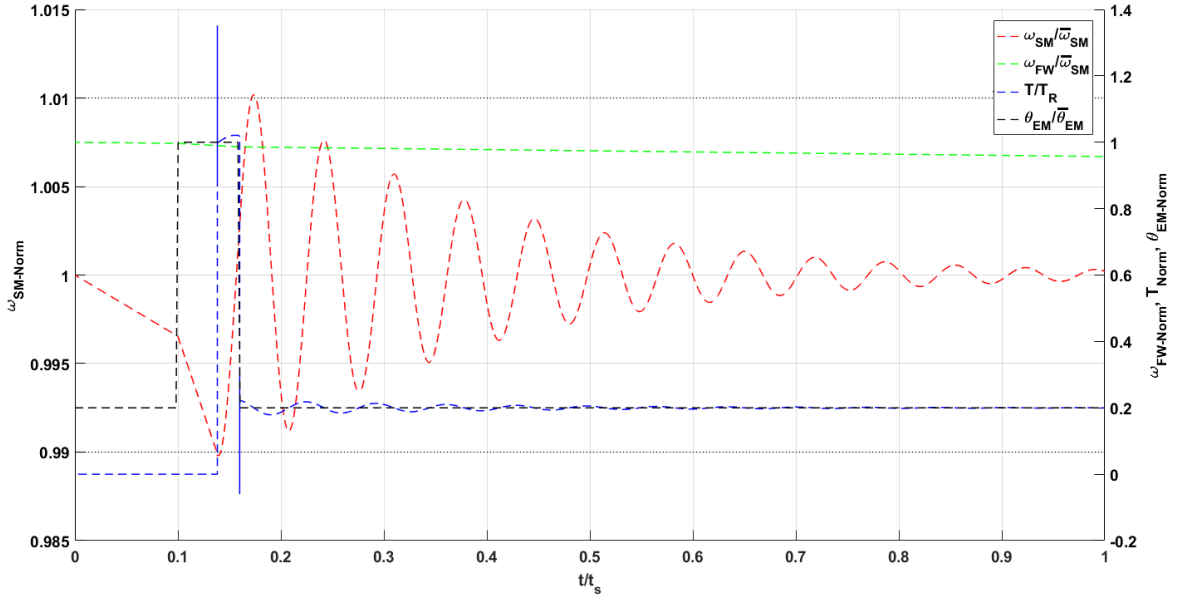

Figure 8: SHyKESS transient response during discharge with a step load change during mode 1 operation. Note that $t_s = 500s$.

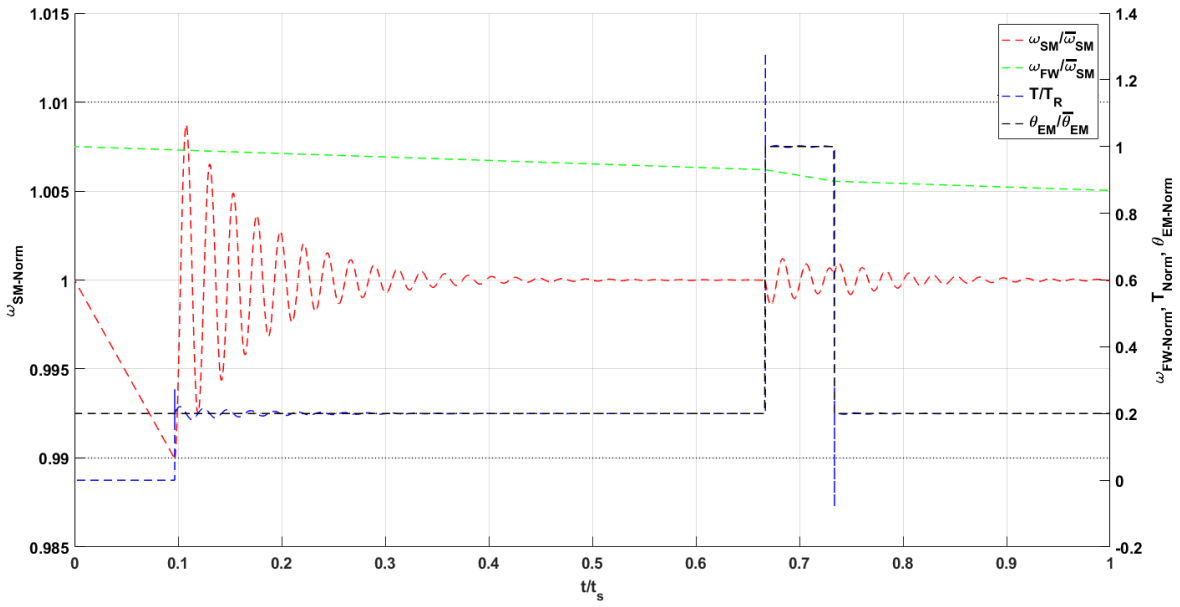

Figure 9: SHyKESS transient response during discharge with a step load change during mode 2A operation. Note that $t_s = 1500s$.

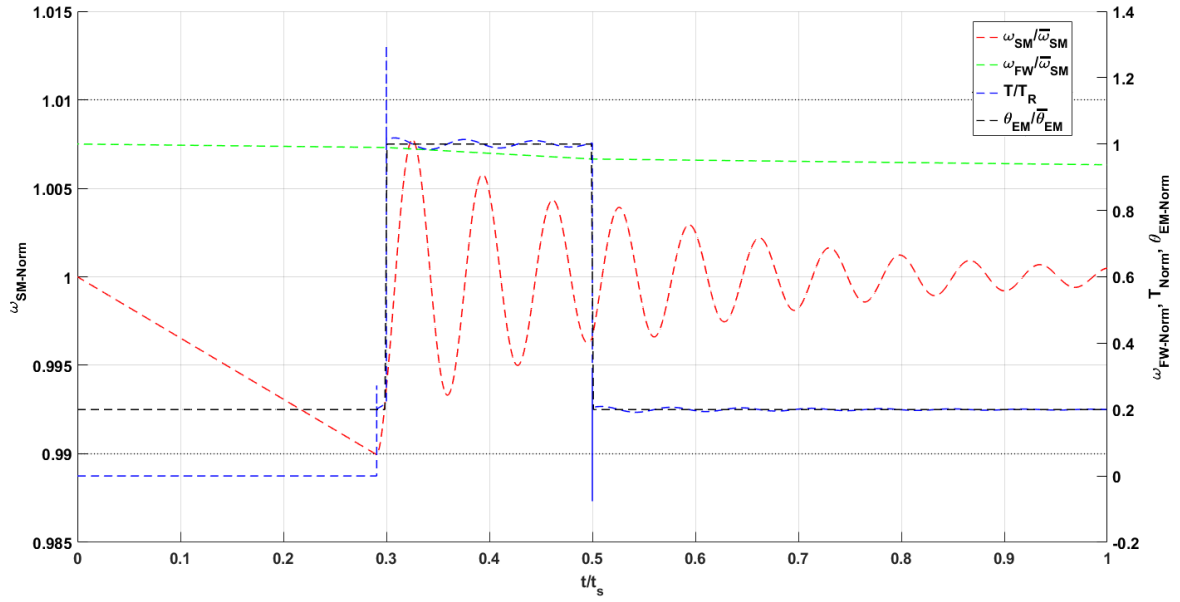

Figure 10: SHyKESS transient response during discharge with a step load change during mode 2A operation (during initial transition settling time). Note that $t_s = 500s$.

6 Comments on Turnaround Efficiency and a Case Study Application of SHyKESS

Determining the turnaround efficiency for the proposed SHyKESS method is difficult due to range of distinct modes that the system may operate in. For example, while operating in mode 1 (as per figure 2), it is foreseeable that the overall system efficiency is governed by the characteristics of the synchronous machine (losses in the flywheel are likely to be minimal[3] and there are, presumably, no

transmission losses if the DDU is locked). It is worth noting here that, due to the size of the system, it is expected that SHyKESS will operate in a vertical orientation supported by magnetic bearings, with rolling element bearings carrying only a small fraction of the rotor load but providing stiffness to the bearing system. Given that most of the rotor load is supported by magnetic bearings, it is reasoned here that bearing losses will be negligible in comparison to other sources.. When the DDU unlocks (in all other modes of operation) efficiency depends on the electric machine, hydraulic machines, and power distribution characteristics; turnaround efficiency is, in the case of SHyKESS, loading history dependent. Before presenting an examination of turnaround efficiency values, approximate models are required that can indicate individual component, namely the synchronous electric machine and hydraulic machine, efficiency levels.

Flywheel systems can be highly efficient. The numerical analyses presented in this section consider the flywheel storage component of SHyKESS to be 100% efficient, however a brief discussion of related losses is given here for completeness and to justify this assumption. It is expected that a flywheel of the dimensions considered in the present work will operate in a vacuum chamber, however the difficulties associated with dynamic sealing make aerodynamic/frictional loss (windage) calculations relevant, with the total loss of operating vacuum representing a "worst case" operating condition.

Windage losses, that is to say the losses related to aerodynamic viscous friction, may be approximated for the wetted sides of a spinning disc using the equations of Daily and Nece[28, 29] (see equations (14) and (15), valid for mixed boundary turbulent flow conditions). A torque due to windage, T_W, can be correlated to the dimensionless coefficient C_W through equation (14). C_W may be calculated using equation (15), where the quantity s/R_O is a ratio of the axial air gap and Re is Reynold's number (given in equation (16)). Using typical values for ambient dry air and assuming a clearance of $0.01m$, losses due to windage at synchronous speed may be estimated as $3884kW$, or 19.42% of the SHyKESS system rated power . It is important to note that this value represents total windage losses due to viscous effects on both wetted end faces of the spinning disc; losses in the radial air gap are not evaluated. High leakage rates associated with this situation are clearly undesirable; losses of $18.65MWh$, almost the total capacity of the flywheel store, may be calculated for a 24 hour period following loss of vacuum.

The observations made above underline the importance of operating in a vacuum for high speed flywheels, however several important points should be noted relating to the above calculation. Firstly, laboratory scale discs used to experimentally validate equations (14) and (15) are typically much smaller than the flywheel sized for SHyKESS. In the work of Etemad et al., for example, a disc of $92mm$ in diameter was considered spinning at a maximum speed of $10472rad/s$[29]. While peripheral speeds are comparable between Etemad's flywheel and the SHyKESS example, Reynold's number values are several orders of magnitude greater for SHyKESS. Equation (15) is empirically determined and its extrapolation to the SHyKESS operating conditions must be acknowledged. Further fundamental work is required in order to properly validate the losses reported above. Secondly, SHyKESS operating under atmospheric conditions would constitute a fault condition. If dynamic sealing can be achieved a vacuum chamber can be established around SHyKESS's flywheel. Hearn et al. note that the development of flywheel energy stores for long term storage has been hampered due to, in part, frictional losses resulting from windage and magnetic bearings, however an operating vacuum of $1mTorr$ has been suggested to address these concerns[30]. If air density values are for corrected for a $1mTorr$ chamber pressure, windage losses drop to $0.15kW$. Self discharge under such conditions is arguably negligible, with a loss in stored energy over a 24 hour period of $3.6 \times 10^{-3} MWh$. This figure may be alternatively expressed as 0.018% of the total storage capacity of the sized SHyKESS flywheel. It is worth noting here that Liu et al.[31] have suggested that low pressure environment windage losses are proportional to the square of angular speed. Magnetic bearing lamination core losses may also be expressed using the same relationship. Functions to define proportionality constants, which are heavily dependent upon flywheel geometry, dimensions, and surface roughness, are however difficult to find in the literature. The model of Daily and Nece has therefore been used to evaluate low pressure windage losses here. Finally, the structure of SHyKESS is such that it may continue to operate through the vacuum chamber fault outlined at the start of this discussion. The secondary energy store provides slip energy to account for the difference between the synchronous machine speed and the flywheel speed. If flywheel self-discharge is high, the point at which the DDU is unlocked and slip energy is introduced occurs sooner, but power may still be injected in to/taken from the grid by SHyKESS. Given that the SHyKESS system is intended to operate in at least a partial vacuum, windage losses have been neglected from the rest of the calculations presented here.

$$T_W = \frac{1}{2} C_W \rho_{Air} \omega^2 R_O^5 \tag{14}$$

$$C_W = \frac{0.062}{(s/R_O)^{0.25} \mathrm{Re}^{0.25}} \tag{15}$$

$$\mathrm{Re} = \frac{\rho_{Air} \omega R_O^2}{\mu_{Air}} \tag{16}$$

Determining the fraction of mechanical work that is converted to electrical power in a synchronous generator is a task that has received a great deal attention in the literature (both in terms of experimental evaluation and analytical modelling) and, to a degree, the exact characteristics depend upon the choice of standard[32]. Loses in these machines are generally categorised into windage/friction, core (exciter), field, stray (eddy current losses in end turn features, for example), and auxiliary system (lubrication/cooling pump requirements, for example) related[33]. Although in depth analytical models have been developed in the literature (for example, in the work of Kerkman et al.[34] and Jiao et al.[35]) these are considered outside the scope of the present work and a simplified semi-empirical model is assumed here. Scalable machine efficiency maps may be found in the work of Stipetic and Goss[36] and suggest that machine efficiencies (of the scale used here, namely 20MW) should vary between 85% at low load to 98% at rated load. For the present work, an alternator/motor model is taken from the work of Notton et al.[37], wherein machine efficiencies are represented by simple polynomials. Equation (17) and equation (18) are used here for generator and motor efficiency expressions, giving rise to η_G and η_M, respectively. These expressions make use of a power fraction argument, $\hat{P}_{SM}$, the ratio of instantaneous electrical power to rated electrical power. Plots of generator and motor efficiencies (with respect to power fraction) can be seen in figure 11 a).

$$\eta_G = \left(\frac{P_{Elec}}{P_{Mech}} \right) = \frac{\hat{P}_{SM}}{\hat{P}_{SM} + 0.00915738 + 0.0797107 \hat{P}_{SM}^2} \tag{17}$$

$$\eta_M = \left(\frac{P_{Mech}}{P_{Elec}} \right) = \frac{\hat{P}_{SM}}{\hat{P}_{SM} + 0.01010391 + 0.00731429 \hat{P}_{SM}^2} \tag{18}$$

Hydraulic pump/motor efficiencies (η_P and η_M, respectively) may be calculated using equations (19) and (20), respectively. These expressions are taken from the work of McCandlish and Dorey[38], who built upon the work of Wilson by introducing linearly variable loss coefficient expressions for flow ($Q_{P/M}$, where subscripts here distinguish pump and motor modes of operation) and torque ($T_{P/M}$) calculations, thereby giving more realistic representations of volumetric and frictional losses in hydraulic machines, respectively. Expressions for $Q_{P/M}$ and $T_{P/M}$ may be seen in equations (21) and (22). These expressions incorporate machine operating conditions and design parameters, namely speed (ω, expressed in rad/s), displacement (D, expressed in cc/rev), working pressure difference between inlet and outlet (ΔP, expressed in bar), and the machine displacement fraction (the fraction of actual displacement to rated machine displacement, assuming a variable displacement machine and identified by x). Considered working fluid properties are dynamic viscosity (μ, here taken to be $0.783 Ns/m^2$[23]) and bulk modulus (B, here taken as $1.71x10^9 N/m^2$[23]), both of which are assumed to be independent of machine operating condition (i.e., they are temperature independent). Note P_{Atmos} is the atmospheric pressure. Loss coefficient (C_s, C_v, and C_f) expressions used here assume a radial piston design machines and are summarised by equations (23) to (25)[38]. Hydraulic machine efficiency maps produced by the above method can be seen in figure 11 b). and c)., for the pump and motor modes, respectively.

$$\eta_P = \frac{100 Q_P \pi}{3 x D \omega} \frac{\Delta P D x}{T_P 2\pi} \tag{19}$$

$$\eta_M = \frac{3 x D \omega}{100 Q_M \pi} \frac{T_M 2\pi}{\Delta P D x} \tag{20}$$

$$Q_{P/M} = \frac{3x\omega D}{100\pi} \mp C_s \frac{30 \times 10^6 \Delta P D}{\pi \mu} \mp \frac{\Delta P \omega D}{1 \times 10^6 B} \left(V_r + \frac{1+x}{2} \right) \tag{21}$$

$$T_{P/M} = \frac{\Delta P D x}{2\pi} \pm C_v \frac{\mu \omega D}{1 \times 10^9 2\pi} \pm C_f \frac{\Delta P D}{2\pi} \tag{22}$$

$$C_s = 1.86 \times 10^{-10} \left(\frac{\Delta P}{P_{Atmos}} \right)^{0.5} \left(0.76 + 0.41 \frac{3\omega}{250\pi} \right) \tag{23}$$

$$C_v = 1.77 \times 10^5 + (4.05 - 1.77) \times 10^5 \left(\frac{x - 0.25}{0.75 - 0.25} \right) \tag{24}$$

$$C_f = 0.031 \left(1 - 0.51 \left(\frac{3\omega}{250\pi} \right) + 0.98 \left(\frac{3\omega}{250\pi} \right)^2 \right) \tag{25}$$

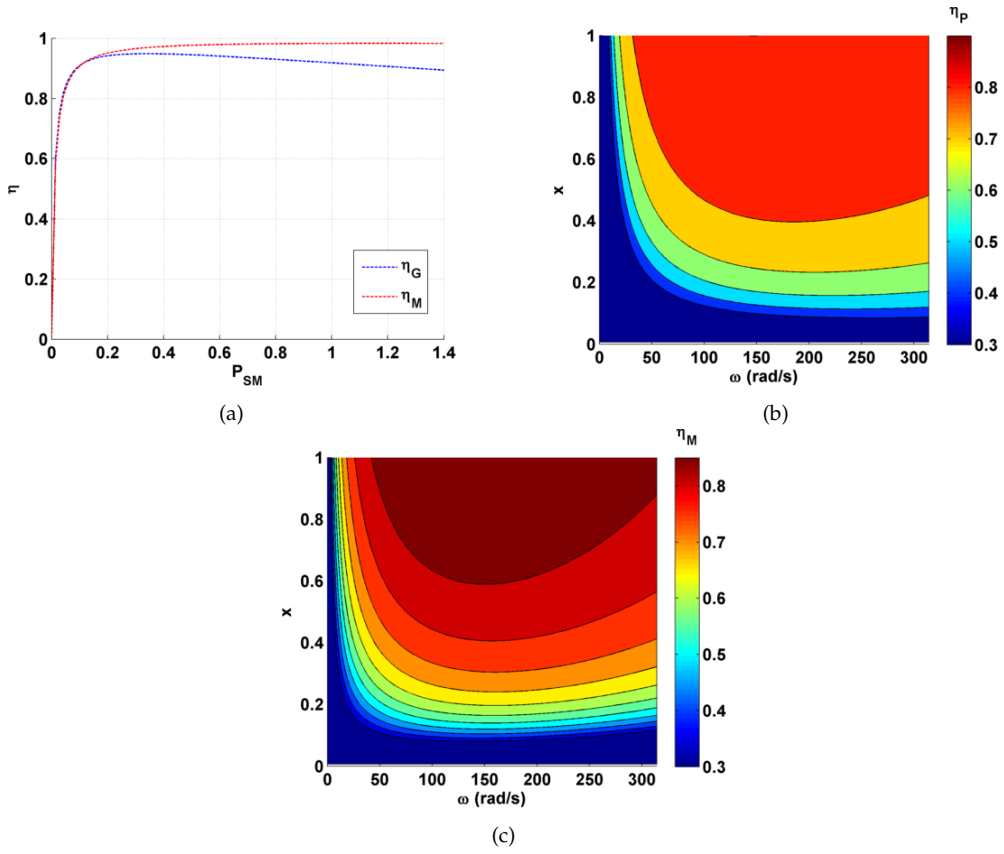

Figure 11: Plots of assumed SHyKESS component efficiency models, showing a). the synchronous machine, operating in as both a generator and a motor (η_G and η_M, respectively), b). the hydraulic machine (pump mode), and c). the hydraulic machine (motor mode).

The turnaround efficiency of SHyKESS can be investigated using the efficiency models for the synchronous and hydraulic machines described above, however some careful consideration is warranted in order to define an appropriate turnaround efficiency metric, remembering that this will almost certainly be dependent upon loading history path. A symmetric discharge/charge loading profile will be assumed in the following discussions, with losses in the flywheel and secondary energy stores evaluated in order to estimate the system efficiency. It is assumed that SHyKESS is initially locked (in mode 1, see figure 2) and is subjected to a sinusoidal loading profile (see equation (26)), where P_L is the instantaneous grid power. Note that the same sign convention is used here as in other sections of the

present work, whereby a positive power indicates a grid demand and necessitates that SHyKESS will be discharged. This allows for the definition of a loading power amplitude (A_L) and period (t_L), which can be used to characterise a wide range of potential grid imbalance scenarios. Turnaround efficiency for SHyKESS (η_T) is defined by equation (27), where ΔE_{FW} is the change in flywheel energy over the loading period and ΔE_{HY} is the change in energy in the secondary store. A "transaction" energy is defined ($E_{Tran} = (2A_L t_L)/\pi$) that quantifies the total amount of energy extracted from/injected into the grid. Equation (27) is judged to be a representative measure of system efficiency (in this case) as it is anticipated that SHyKESS will typically operate at relatively low slip speeds and around synchronous speed. Self discharge of the flywheel is assumed to be negligible, allowing the system can remain in a charged and locked state for long periods of time. A detailed discussion of this point may be found in the conclusions section of this paper, however it should be noted that additional fundamental work is required to determine windage losses, for example, in systems on the scale of SHyKESS before enhanced efficiency maps can be created. SHyKESS turnaround efficiency is plotted in equation (27), with respect to loading amplitude (A_L) and period (t_L).

$$P_L(t) = A_L \sin\left(\frac{t}{t_L} 2\pi\right) \tag{26}$$

$$\eta_T = 1 - \frac{|\Delta E_{FW}| + |\Delta E_{HY}|}{E_{Tran}} \tag{27}$$

Several interesting features can be noted from figure 12 which illuminate certain subtle aspects of SHyKESS operation. For very low values of t_L turnaround efficiencies are typically high (over 0.8). At low depths of discharge/charge SHyKESS efficiency is almost entirely determined by the synchronous machine; the DDU remains locked (mode 1) and all power is extracted from/injection into the flywheel. Note a lower threshold value of 0.85 is applied to the electric machine in the current work to avoid difficulties associated with electrical machines operating at low power fractions. Similarly, a lower efficiency threshold of 0.3 is applied to the hydraulic machine. It is easy to imagine that as A_L increases in magnitude the time at which the DDU will unlock (moving from mode 1 into mode 2 operation) will reduce. As t_l increases therefore (for a given value of A_L), a great proportion of power must be supplied through the DDU (that is to say, from the secondary store) during the loading cycle. Although, generally speaking, operating the hydraulic machine at higher speeds and closer to rated power results in larger component efficiencies, the fact remains the energy transactions in this range of operation experience losses in both the synchronous machine and hydraulic machine, leading to reductions in η_T for an increase in t_L. These effects may be readily observed in figure 12 when A_L is greater than $20MW$.

When $A_L < 20MW$ a drop off in η_T is observed, with a region of particularly low efficiency values for high t_L (see the bottom right hand corner of figure 12). Such behaviour can be explained by considering how the hydraulic machine "moves" through the efficiency maps presented in figure 11 b). and c). during a discharge/charge cycle. For a constant load condition (which is easier to consider for the present discussion than the sinusoidal profile used in figure 12), hydraulic machine efficiency follows a linear path along a diagonal, the bearing of which is determined by the magnitude of the system load. Initially, slip speeds are small and only a small fraction of the load power is supplied by the hydraulic machine (as far as the present discussion is concerned, this can be thought of as x in figure 11 b). and c).). Returning attention to the sinusoidal loading patterns, higher values of A_L allow for the larger values hydraulic machine efficiency to be exploited (the machine operates closer to its rated value for a greater portion of the loading cycle). For comparatively low values of A_L however the hydraulic machine power is consistently low compared to the machine's rated value, resulting in low machine efficiencies. Similar effects can be observed in the synchronous machine (i.e. when it operates at a low power fraction), thereby leading to relatively low values of η_T when the DDU unlocks at low A_L values. At very low values of A_L, η_T is almost completely independent of t_L as the depth of discharge/charge is not sufficient to unlock the DDU over the loading period. It should be recalled that windage losses have not been consider in the generation of figure 12. These additional losses, which at most amount to $660kW$, are likely to have little influence at high A_L values, where the flywheel store is quickly discharged and DDU unlocks relatively early in the simulation. At lower A_L values windage is expected to have a significant effect as its magnitude is similar to that of the peak transaction power. This observation further indicates why SHyKESS may not be suitable for use in low partial load conditions.

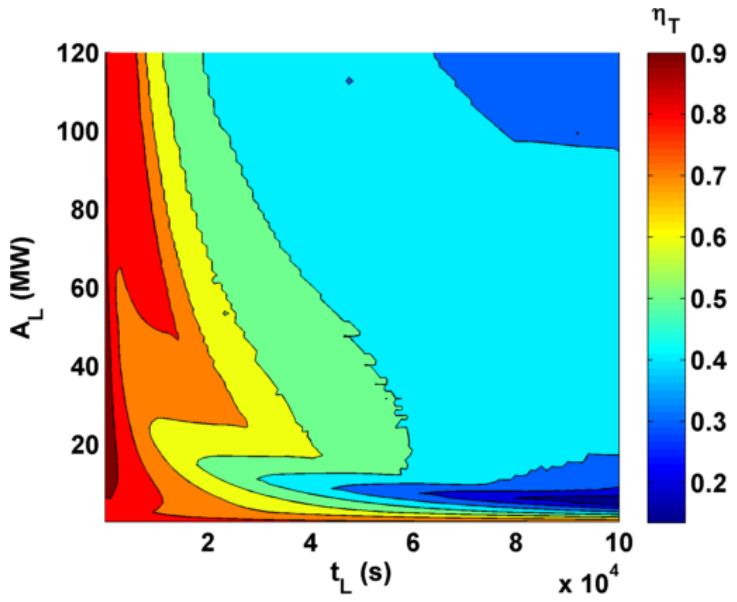

Figure 12: The derived SHyKESS efficiency map (for sinusoidal supply/demand loading conditions).

In order to demonstrate the applicability of SHyKESS and it's ability to reinstate real inertia in grids where it has been removed, we here present a simple case study for an isolated grid that has a baseline supply which is augmented by a photovoltaic (PV) power station (which has little intrinsic real inertia). A fictional Californian grid is considered here in order to provide a suitable setting for a PV power station.

A PV cell model is implemented here that is based on the work Durisch et al. A semi-empirical efficiency model was developed in this work and verified against observations made in Jordan (Al Quawairah)[39] over a three year period[40], with further comparisons made against Californian and Alpine data (making its application in the present case study appropriate). The developed efficiency model is summarised by equation (28), where the parameters h_{PV} (the Ross coefficient[39]), p_{PV}, q_{PV}, m_{PV}, r_{PV}, s_{PV}, and u_{PV} are manufacturer/model specific. In the present work, a Siemens CIS ST40 copper-indium-diselenide ($CuInSe_2$) is adopted, for which the parameters presented in table 2 may be assumed (note individual modules have an area, A, of $0.423m^2$). Note that in equation (28), G_β is the global solar irradiation, θ_{PV} is the panel temperature, and M_{Air} is a (normalised) air mass. For reference, a typical working efficiency of the selected PV module (where $600W/m^2 \leq G_\beta \leq 800W/m^2$, $\theta_{pv} = 25^oC$, and $M_{Air} = 1.5$) is approximately 12%[39]. Several site specific meteorological variables (namely global solar irradiation, G_β, air temperature, θ_{Air}), and normalised air mass, M_{Air}, must be defined in order for equation (28) to be implemented. Some attention will now be given to appropriate models that described these parameters in California.

Table 2: Assumed Durisch model PV cell parameters for a Siemens CIS ST40 $CuInSe_2$ module[39].

Parameter	Value
$h_{PV}(^oC.m^2/W)$	0.032
p_{PV}	0.1855
q_{PV}	-0.3288
m_{PV}	0.2612
r_{PV}	-0.10039
s_{PV}	-0.9678
u_{PV}	0.9864

$$\eta_{PV} = p_{PV}\left(q_{PV}\frac{G_\beta}{G_{\beta,0}} + \left(\frac{G_\beta}{G_{\beta,0}}\right)^{m_{PV}}\right)\left(1 + r_{PV}\frac{\theta_{PV}}{\theta_{PV,0}} + s_{PV}\frac{M_{Air}}{M_{Air,0}} + \left(\frac{M_{Air}}{M_{Air,0}}\right)^{u_{PV}}\right) \tag{28}$$

Solar irradiance is modelled here using the work of Sung et al., which was validated against data taken from Anatolia-Rancho Cordova, California[41]. This model allows for both long and short term weather induced variations, see equations (29) and (30). In these equations, I_{ETI} is the maximum extraterrestrial solar irradiation, d_n is the day within the year (samplings in mid July are considered here), ψ_z is the zenith angle (in degrees), t is a specific time in the day (expressed in hours), t_{rise} is the sunrise time, and t_{set} in the sun set time. The following model parameters are assumed to be representative of California, $M = 0.76$, $a_1 = 0.1$, $b_1 = 7$, $c_1 = 1$, $a_2 = 0.5$, $b_2 = 40$, $c_2 = 2$, and $d_n = 180$[41].

$$G_\beta = S_{max} \sin\left(\frac{\pi\left(t - t_{rise}\right)}{t_{set} - t_{rise}}\right)\left(1 - a_1\left|\sin\left(b_1\frac{\pi\left(t - t_{rise}\right)}{t_{set} - t_{rise}}\right)\right|^{c_1} - a_2\left|\sin\left(b_2\frac{\pi\left(t - t_{rise}\right)}{t_{set} - t_{rise}}\right)\right|^{c_2}\right) \tag{29}$$

$$S_{max} = M\max\left(I_{ETI}\right) = M\max\left(1362\left(1 + 0.033\cos\left(\frac{2\pi d_n}{365}\right)\right)\cos\left(\psi_z\right)\right) \tag{30}$$

PV cell temperature (θ_{PV}) is assumed to be governed by $\theta_{PV} = \theta_{Air} + h_{PV}G_\beta$, where h_{PV} is the Ross coefficient (see table 2). An approximation of daily air temperature variations is now required and is here based on the work of Cesaraccio et al. (particularly related to the Calipatria weather station in California)[42]. The TM model splits diurnal temperature variations into three regions, based on time of day relative to sun rise and sun set (each controlled by a function, see equation (31)). In this model, $\hat{\theta}_{Air}$ is the peak air temperature during the day (occurring at the time $t_{\hat{\theta}_{Air}}$), $\theta_{Air,n}$ is the air temperature at t_{rise} ($\theta_{Air,p}$ is the air temperature at t_{rise} the following day; it is assumed here that $\theta_{Air,p} = \theta_{Air,n}$), and $\theta_{Air,o}$ is the air temperature at t_{set}. A summary of assumed parameters used for air temperature modelling (and solar irradiance modelling) can be found in table 3 (note that these are largely taken from the work of Cesaraccio et al.[42]). Note that, in the three phases of equation (31), the following substitutions are used; $\alpha = \hat{\theta}_{Air} - \theta_{Air,n}$, $R = \hat{\theta}_{Air} - \theta_{Air,o}$, and $b = \left(\theta_{Air,p} - \theta_{Air,o}\right) / \left(\sqrt{t_{rise} - t_{set}}\right)$.

Table 3: A summary of parameters used the solar irradiance and air temperature modelling (representative of California).

Parameter	Value
$\hat{\theta}_{Air}(^oC)$	31.0
$\theta_{Air,n}(^oC)$	13.8
$\theta_{Air,o}(^oC)$	25.0
t_{rise}	06 : 00
$t_{\hat{\theta}_{Air}}$	13 : 00
t_{set}	20 : 30

$$\theta_{Air}(t) = \begin{cases} \theta_{Air,n} + \alpha\sin\left[\left(\dfrac{t - t_{rise}}{t_{\hat{\theta}_{Air}} - t_{rise}}\right)\dfrac{\pi}{2}\right], & \text{if } t_{rise} < t \leq t_{\hat{\theta}_{Air}} \\ \theta_{Air,o} + R\sin\left[\dfrac{\pi}{2} + \left(\dfrac{t - t_{\hat{\theta}_{Air}}}{t_{set} - t_{\hat{\theta}_{Air}}}\right)\dfrac{\pi}{2}\right], & \text{if } t_{\hat{\theta}_{Air}} < t \leq t_{set} \\ \theta_{Air,o} + b\sqrt{t - t_{set}}, & \text{if } t_{set} < t \leq t_{rise} \end{cases} \tag{31}$$

Normalised air mass (M_{Air}) is correlated to ψ_z (zenith angle) through Notton's interpretation[43, 37] of Kasten and Young's revised air mass tables[44] (see equation (32)).

$$M_{Air} = \frac{1}{\cos\left(\psi_z\right) + 0.50572\left(96.07995 - \psi_z\right)^{-1.6364}} \tag{32}$$

Finally, inverter efficiency for the PV cell is based on a model used extensively by Notton et al.[43, 37] (see equations (33) to (35)), where $\eta_{10} = 0.87$ and $\eta_{100} = 0.945$. Note that $\hat{P}$ is the ratio of the inverter output power to the rated inverter power.

$$\eta_{INV} = \frac{\hat{P}}{\left(\hat{P} + P_0 + k\hat{P}\right)^2} \tag{33}$$

$$P_0 = \frac{1}{99}\left(\frac{10}{\eta_1 0} - \frac{1}{\eta_{100}} - 9\right) \tag{34}$$

$$k = \left(\frac{1}{\eta_{100}}\right) - P_0 - 1 \tag{35}$$

Using the PV model (and related equations) expressed above, a PV cell's response in California may be approximated. A plot of the daily variations in air temperature (θ_{Air}), extraterrestrial solar irradiance (I_{ETI}), global solar irradiance (G_β), and PV cell output power (after the inverter, P_{PV}) can be seen in figure 13 a). which was generated assuming the California representative parameters reported in the present work. A scaled demand profile (P_{Demand}) has been assumed to be representative of a Californian grid (see figure 13 b).). Assuming a baseline load (P_{Base}, here taken to be the first 15 terms in a Fourier decomposition of the demand signal, representing temporal frequencies between $1.6534 \times 10^{-6} Hz$ and $2.4802 \times 10^{-5} Hz$) and superimposing the PV power station generation ($P_{PV,Total}$), temporally varying supply (P_{Gen}) and demand (P_{Demand}) fluctuations may be generated (see figure 14 a).). Inspection of these profiles has identified three loading events which are interest to SHyKESS (i.e. cases where there are short term energy imbalances which may be extended into the long term). These are summarised in figure 14 b)., c)., and d). (in subsequent discussions these will be referred to as events 1, 2, and 3, respectively). Transient SHyKESS responses are plotted for the three loading events (assuming the same $50MW$ $20MW.Hr$ design discussed previously) in figures 15 to 17 (note the same normalisation convention is used as in section 5). It should be noted that, in all cases, SHyKESS initially presents a high inertia to the grid in order to limit the rate of change of frequency and, after the DDU unlocks, the simple PID controller is sufficient to return the frequency back to it nominal operating value (this is the case even when presented with loading patterns that are representative of real grids). These results indicate that SHyKESS is suitable for controlling grid frequency over a wide range of time scales, with a significant amount of power being provided by a flywheel in all cases.

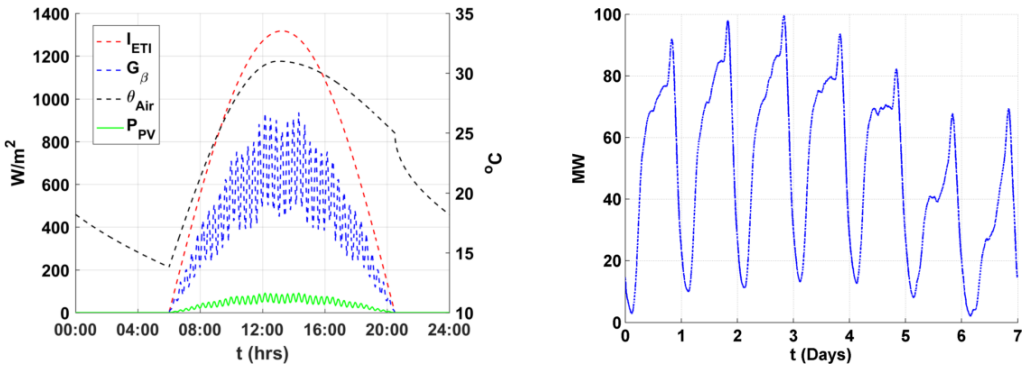

(a) (b)

Figure 13: Plots of a). generated diurnal solar panel response (P_{PV} based on a Siemens CIS ST40 $CuInSe_2$ in California, USA, in July) per unit area and related parameters and b). the assumed demand profile.

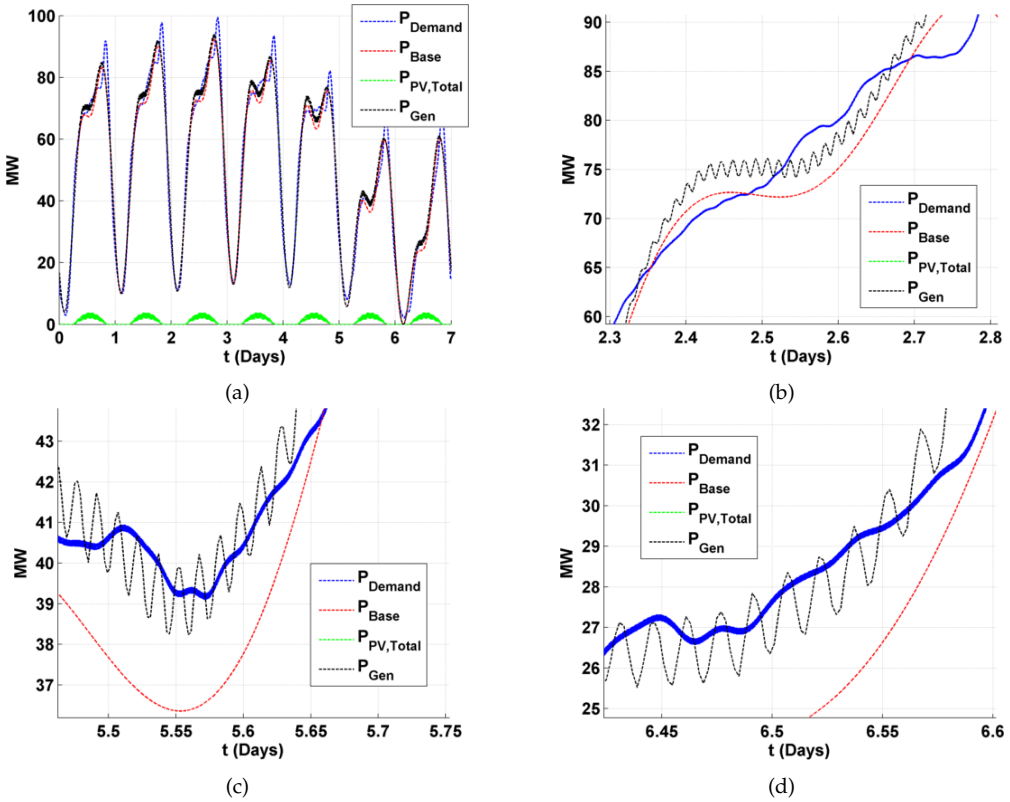

Figure 14: Plots of a). the generated power supply and demand profiles (with constitutive baseline and PV components plotted independently), b). identified case study event 1, c). identified case study event 2, and c). identified case study event 3.

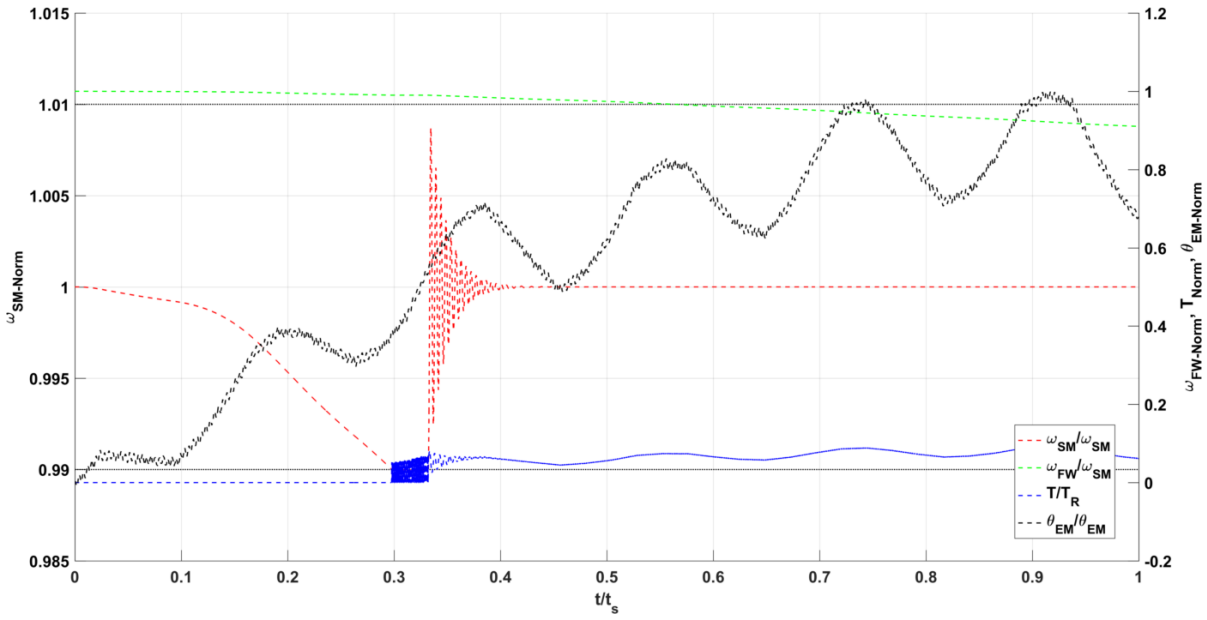

Figure 15: SHyKESS transient response for event 1 (see figure 14).

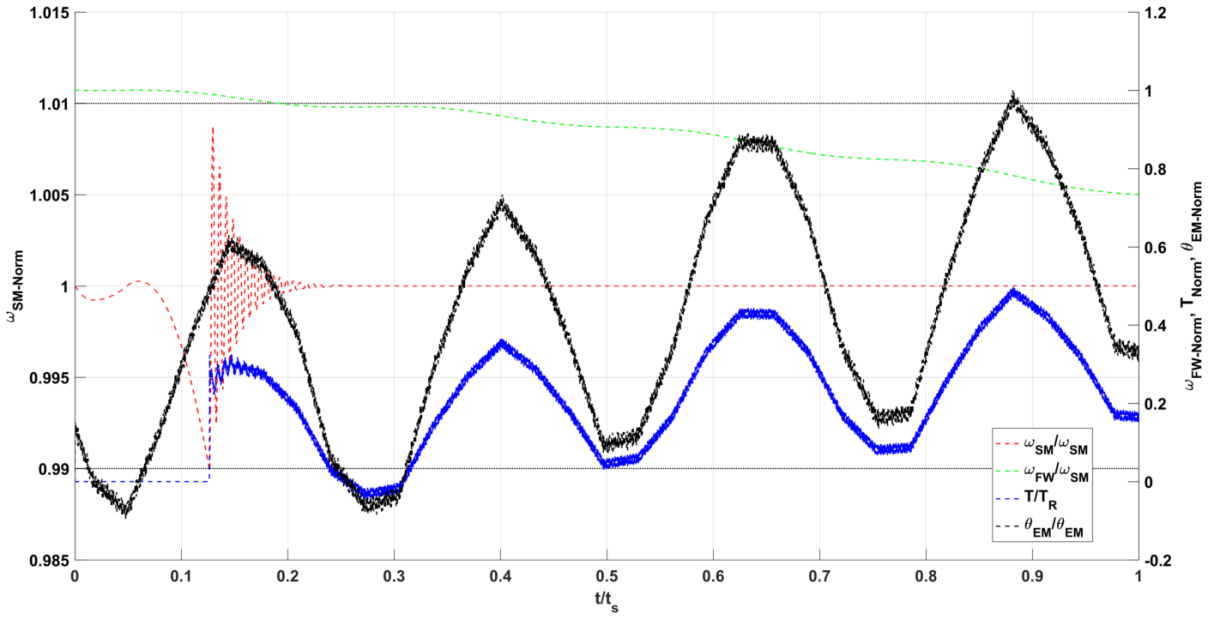

Figure 16: SHyKESS transient response for event 2 (see figure 14).

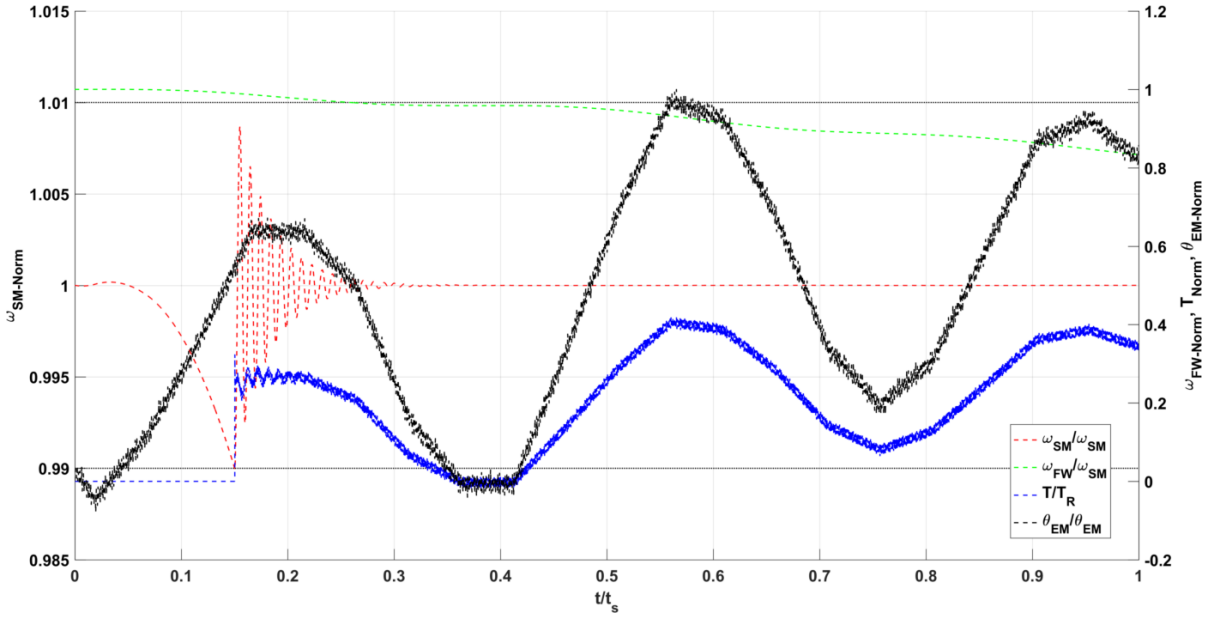

Figure 17: SHyKESS transient response for event 3 (see figure 14).

7 Conclusions and Future Work

Replacing system inertia in a decarbonised energy market has been identified by many parties as an area that needs investment. A hybrid energy storage system (SHyKESS) is presented here that incorporates 2 energy stores (facilitating both fast and slow energy storage) which attempts to address this issue. The use of flywheel energy storage is attractive due to the inherently high levels of inertia, however flywheels also benefit from high cycle and operational lives, high turnaround efficiencies, high energy densities and low environmental impacts [15, 45]. The proposed system belongs to the electricity in/electricity out class of stores and is built on a hollow shaft in such a way that torque is not explicitly grounded to earth. As such, losses in the system may be minimised and the support structures reduced (i.e. reaction torques

through component casings are minimised). An example $50MW$ system with $20MWh$ of capacity has been sized and simulated, with appropriate gain levels found for a PID controller that dictates the power contributions from both energy stores in certain modes of operation. Simulations considered both idealised step loading histories and grid representative examples and, in all cases, synchronous machine speeds remained within industry accepted tolerances; this could be realised with in a system with only normal (i.e. thermal power plant) levels of power electronics. No frequency control power electronics are required. Large inertia constants may be calculated ($1440s$ for the developed system) and, during certain mode of operation, there is no ambiguity as to whether this inertia is "seen" by the grid. Assuming steel prices of £$2000/tonne$, unit energy storage costs of approximately $111.5£/kW.hr$ are achievable with this system. Almost no cyclic degradation would be expected and control (when required) can be both simple and localised (the system is intrinsically un-hackable and is resistant to cyber attack). Furthermore, the inclusion of a synchronous machine in SHyKESS offers an advantage over power electronics controlled synthetic inertia systems. Power electronics are often sized based on a nominal power and are not suited to operating in overload conditions for extended periods of time (typically on the millisecond time scale). Synchronous machines on the other hand can typically be operated at overrated power levels for several seconds before thermal and strucutral concerns limit continued operation. It is foreseeable that, under fault conditions, high current levels would be required such that faults could be cleared or system protection could take effect. The flexibility that a system such as SHyKESS would offer during both normal operating and fault conditions is an interesting feature of hybrid energy stores that incorporate synchronous machines. Future work will look to explore this area in detail.

The modelling procedure implemented here has used a first order approximation of a synchronous machine. A constant field strength is assumed, allowing the machine to be approximated by a constant stiffness rotational spring. While this has been judged to be sufficient for the present work (the main objective in here is to introduce the SHyKESS concept and illustrate how such a system can operate in several modes), this issue must be addressed in future work. Furthermore, refined efficiency models for the electric and hydraulic machines should be investigated, particularly with reference to start up conditions.

Numerous novel flywheel designs have been proposed which could form part of a SHyKESS design and will be investigated. For example, integrated flywheel, motor/generator and magnetic bearing systems in the work of Kailasan et al.[46] benefited from reduced shaft lengths. Additional flexibility in the design is present through the choice of flywheel and transmission shaft materials[47] and shape of the flywheel (for example, the use of constant stress flywheel cross sections with or without an outer retaining ring[47]), which are generally characterised by the shape factor K[48]. Of particular note will be the development of low leakage rotating unions that can accommodate the intended working pressures ($200bar$) of the compressed fluid store.

Flywheel sizing in the present work was conducted using an elastic-perfectly-plastic material (approximating EN24 steel) and assuming a Tresca yield criterion. The validity of this solution was questioned in the work of Gamer[49] due to non-continuous displacement field solutions in partial plasticity cases and negative radial plastic strains (associated with tensile radial stresses) for solid disc applications (ar the centre of the disc is considered). In order to address these points, Gamer developed a solution using a Prager hardening rule (linear kinematic hardening) which still implemented the Tresca criterion. More recently, solutions using a von Mises criterion have been found[50]. The exact implications of these refinements on the flywheel design is presently unclear and future work should look to quantify the potential for design enhancements.

By fluctuating rotational speed, tensile stresses experienced in flywheels will also fluctuate, meaning that fatigue becomes a legitimate life limiting failure mechanism. This observation is particularly true in the case of SHyKESS, where the extended operational range made possible by the DDU offers the potential for a larger alternating stresses. A brief examination of this failure mechanism is given here using the Basquin model, which is summarised by equation (36). In equation (36), α and β are material/surface condition dependent parameters which relate the number of cycles to failure N_f to the "endurance" alternating stress $\Delta\sigma$ for fully reversed conditions. Values for α and β are here taken as 9.84 and 4.56×10^{30}, respectively, being representative of a smooth surface component made from medium carbon steel (similar to the EN24 material referenced above)[51]. Equation (36) is only valid for fully reversed, or 0 mean stress, loading conditions, therefore the well known Goodman relationship must be used to account for mean stress effects. The Goodman relationship may be expressed by equation (37),

where S_A and S_M are the alternating and mean stresses for a particular loading condition, respectively, σ_e is the endurance limit for a given number of cycles to failure, here calculated by equation (36), and σ_{UTS} is the ultimate tensile strength of the material, here taken to be $2000MPa$. Attention is restricted in the present discussion to an extended discharge of flywheel loading pattern, wherein the flywheel operates between synchronous speed and a 50% charged state. Using equations (7) to (9) stresses in the hoop direction may be calculated for these conditions, yielding a result that $S_A = 295MPa$ and $S_M = 885MPa$. Substituting these values into equation (37) indicates a required endurance stress of $529MPa$. From equation (36), these conditions suggest a failure life of approximately 7200 cycles. The above is a first order calculation which extends methods that are usually reserved for high cycle fatigue calculations into scenarios where low cycle methods may be more appropriate. What is revealed however are the potentially significant fatigue effects which can limit the life of flywheel components, particularity if designs which look to utilise material effectively are sought. Future work will explore these limitations more closely and will look to account for variable loading cycles through damage summation methods such as Miners rule.

$$\Delta\sigma^{\alpha} N_f = \beta \tag{36}$$

$$S_A = \sigma_e \left(1 - \frac{S_M}{\sigma_{UTS}}\right) \tag{37}$$

As discussed in section 4, the flywheel considered in the present work is expected to be made up of several plates which are held axially. This helps to avoid several major manufacturing and logistic challenges, however it does necessitate the inclusion of additional features in the flywheel which may act as locations of stress concentration. Future work will look to clarify the nature of these features and determine the likelihood of premature failure due to their inclusion.

8 Acknowledgements

The presented work is funded by the EPSRC (EP/R001251/1) and incorporates collaborations with the Energy Technologies Institute (ETI), Power Continuity Systems and Quartzelec Ltd.

References

[1] Sørensen, B . Energy Intermittency. CRC Press; 2014.

[2] Jain P. Wind Energy Engineering. McGraw Hill; 2010.

[3] Díaz-González F, Sumper A, Gomis-Bellmunt O. Energy Storage in Power Systems. Wiley; 2016.

[4] Keyhani A, Marwali MN, Dai M. Integration of Green and Renewable Energy in Electric Power Systems. Wiley; 2010.

[5] Bassi F, Caciolli L, Giannuzzi G, Corsi N, Giorgi A. Use of Hidden Inertia from Wind Generation for Frequency Support in Power Grids. In: AEIT International Annual Conference (AEIT), 2016; 2016. .

[6] Kothari DP, Nagrath IJ. Modern Power System Analysis. McGraw-Hill Education; 2003.

[7] Dreidy M, Mokhlis H, Mekhilef S. Inertia Response and Frequency Control Techniques for Renewable Energy Sources: A Review. Renewable and Sustainable Energy Reviews. 2017;69:144–155.

[8] Deepak M, Abraham RJ, Gonzalez-Longatt FM, Greenwood DM, Rajamani HS. A Novel Approach to Frequency Support in a Wind Integrated Power System. Renewable Energy. 2017;108:194–206.

[9] Jiebei Zhu GPAAJR Campbell D Booth, Bright CG. Inertia Emulation Control Strategy for VSC-HVDC Transmission Systems. IEEE Transactions on Power Systems. 2013;28:1277–1287.

[10] Pipelzadeh Y, Chaudhuri B, Green TC. Inertial Response from Remote Offshore Wind Farms Connected through VSC-HVDC Links: A Communication-less Scheme. In: Power and Energy Society General Meeting, 2012 IEEE; 2012. .

[11] Prodromidis GN, Coutelieris FA. Experimental and Theoretical Investigation of Flywheel-Based Energy Storage in Off-Grid Power Plants Using Renewables. Journal of Energy Engineering. 2016;142:04014055–1–8.

[12] Prodromidis GN, Coutelieris FA. Simulations of Economical and Technical Feasibility of Battery and Flywheel Hybrid Energy Storage Systems in Autonomous Projects. Renewable Energy. 2012;39:149–153.

[13] Sebastián R, Peña Alzola R. Control and Simulation of a Flywheel Energy Storage for a Wind Diesel Power System. Electrical Power and Energy Systems. 2015;64:1049–1056.

[14] Carrillo C, Feijóo A, Cidrás J. Comparative Study of Flywheel Systems in an Isolated Wind Plant. Renewable Energy. 2009;34:890–898.

[15] Amiryar ME, Pullen KR. A Review of Flywheel Energy Storage System Technologies and their Applications. Applied Sciences. 2017;7:1–21.

[16] Sebastián R, Peña Alzola R. Flywheel energy storage systems: Review and simulation for an isolated wind power system. Renewable and Sustainable Energy Reviews. 2012;16:6803–6813.

[17] Amrouche SO, Rekioua D, Rekioua T, Bacha S. Overview of Energy Storage in Renewable Energy Systems. International Journal of Hydrogen Energy. 2016;41:20914–20927.

[18] Bocklisch T. Hybrid Energy Storage Systems for Renewable Energy Applications. Energy Procedia. 2015;73:103–111.

[19] Shankar G, Mukherjee V. Load Frequency Control of an Autonomous Hybrid Power System by Quasi-oppositional Harmony Search Algorithm. International Journal of Electrical Power and Energy Systems. 2016;78:715–734.

[20] Hamzaoui I, Bouchafaa F, Talha A. Advanced Control for Wind Energy Conversion Systems with Flywheel Storage Dedicated to Improving the Quality of Energy. International Journal of Hydrogen Energy. 2016;41:20832–20846.

[21] Government U. The Electricity Safety, Quality and Continuity Regulations 2002;. Available from: `http://www.legislation.gov.uk/uksi/2002/2665/pdfs/uksi_20022665_en.pdf`.

[22] Hameer S, van Niekerk JL. A Review of Large-scale Electrical Energy Storage. International Journal of Energy Research. 2015;39:1179–1195.

[23] Hunt T, Vaughan N. Hydraulic Handbook. Elsevier; 1996.

[24] Rees DWA. The Mechanics of Solids and Structures. Imperial College Press; 2016.

[25] Rees DWA. Elastic-Plastic Stresses in Rotating Discs by von Mises and Tresca. Journal of Applied Mathematics and Mechanics. 1999;79:281–288.

[26] RoyMech;. Available from: `http://www.roymech.co.uk/Useful_Tables/Matter/Strength_st.htm`.

[27] Klempner G, Kerszenbaum I. Handbook of Large Turbo-Generator Operation and Maintenance, 2nd Edition. Wiley; 2008.

[28] Daily JW, Nece RE. Chamber Dimension Effects on Induced Flow and Frictional Resistance of Enclosed Rotating Disks. Transactions of ASME, Journal of Basic Engineering. 1960;82:217–232.

[29] Etemad MR, Pullen K, Besant CB, Baines N. Evaluation of Windage Losses for High-Speed Disc Machinery. Proceedings of the Institute of Mechanical Engineers. 1992;206:149–157.

[30] Hearn CS, Lewis MC, Pratap SB, Hebner RE, Uriarte FM, Chen D, et al. Utilization of Optimal Control Law to Size Grid-Level Flywheel Energy Storage. IEEE Transactions on Sustainable Energy. 2013;4:611–618.

[31] Liu HP, Werst MD, Hahne JJ, Bogard D. Investigation of Windage Splits in an Enclosed Test Fixture Having a High Speed Composite Rotor in Low Air Pressure Environments. In: 12th Symposium on Electromagnetic Launch Technology; 2004. .

[32] Sumper A, Baggini A. Electrical Energy Efficiency: Technologies and Applications. Wiley; 2012.

[33] Cathey JJ. Electric Machines: Analysis and Design Applying MATLAB. McGraw-Hill Inc.; 2001.

[34] Kerkman RJ, Krause PC, Lipo TA. Simulation of a Synchronous Machine with an Open Phase. Electric Machines & Power Systems. 1977;1:245–254.

[35] Jiao N, Liu W, Pang J, Zhang Z, Jiang Y. Integrated Model of Brushless Wound-Rotor Synchronous Starter-Generator Based on Improved Parametric Average-Value Model of Rotating Rectifier. International Journal of Electrical Power & Energy Systems. 2018;96:106–113.

[36] Stipetic S, Goss J. Calculation of Efficiency Maps using Scalable Saturated Flux-Linkage and Loss Model of a Synchronous Motor. In: 22nd International Conference on Electrical Machines, ICEM 2016; 2016. .

[37] Notton G, Mistrushi D, Stoyanov L, Berberi P. Operation of a Photovoltaic-Wind Plant with a Hydro Pumping-Storage for Electricity Peak-Shaving in an Island Context. Solar Energy. 2017;157:20–34.

[38] McCandlish D, Dorey RE. The Mathematical Modelling of Hydrostatic Pumps and Motors. Proceedings of the Institution of Mechanical Engineers, Part B: Journal of Engineering Manufacture. 1984;198B:165–174.

[39] Durisch W, Bitnar B, Mayor JC, Kiess H, Lam KH, Close J. Efficiency Model for Photovoltaic Modules and Demonstration of its Application to Energy Yield Estimation. Solar Energy Materials & Solar Cells. 2007;91:79–84.

[40] Durisch W, Keller J, Bulgheroni W, Keller L, Fricker H. Solar Irradiation Measurements in Jordan and Comparisons with Californian and Alpine data. Applied Energy. 1995;52:111–124.

[41] Sung T, Yoon SY, Kim KC. A Mathematical Model of Hourly Solar Radiation in Varying Weather Conditions for a Dynamic Simulation of the Solar Organic Rankine Cycle. Energies. 2015;8:7058–7069.

[42] Cesaraccio C, Spano D, Duce P, Snyder RL. An Improved model for Determining Degree-Day Values from Daily Temperature Data. International Journal of Biometeorology. 2001;45:161–169.

[43] Notton G, Lazarov V, Stoyanov L. Optimal Sizing of a Grid-Connected PV System for Various PV Module Technologies and Inclinations, Inverter Efficiency Characteristics and Locations. Renewable Energy. 2010;35:541–554.

[44] Kasten F, Young T. Revised Optical Air Mass Tables and Approximation Formula. Applied Optics. 1989;28:4735–4738.

[45] Mousavi G SM, Faraji F, Majazi A, Al-Haddad K. A Comprehensive Review of Flywheel Energy Storage System Technology. Renewable and Sustainable Energy Reviews. 2017;67:477–490.

[46] Kailasan A, Dimond T, Allaire P, Sheffler D. Design and Analysis of a Unique Energy Storage Flywheel System - An Integrated Flywheel, Motor/Generator, and Magnetic Bearing Configuration. Journal of Engineering for Gas Turbines and Power. 2015;137:042505–1–9.

[47] Huggins RA. Energy Storage. Springer; 2010.

[48] Bolund B, Bernhoff H, Leijon M. Flywheel Energy and Power Storage Systems. Renewable and Sustainable Energy Reviews. 2007;11:235–258.

[49] Gamer U. Tresca's Yield Condition and the Rotating Disk. Journal of Applied Mechanics. 1983;50:676–678.

[50] Aleksandrova N. Exact Deformation Analysis of a Solid Rotating Elastic-Perfectly-Plastic Disk. International Journal of Mechanical Sciences. 2014;88:55–60.

[51] Li C, Dai W, Duan F, Zhang Y, He D. Fatigue Life Estimation of Medium-Carbon Steel with Different Surface Roughness. Applied Sciences. 2007;7.